

Dynamical model of coherent pion production in neutrino-nucleus scatteringS. X. Nakamura,^{1,*} T. Sato,² T.-S. H. Lee,³ B. Szczerbinska,⁴ and K. Kubodera⁵¹*Instituto de Física, Universidade de São Paulo, C.P. 66318, 05315-970 São Paulo, SP, Brazil*²*Department of Physics, Osaka University, Toyonaka, Osaka 560-0043, Japan*³*Physics Division, Argonne National Laboratory, Argonne, Illinois 60439, USA*⁴*Dakota State University, College of Arts & Sciences, Madison, SD 57042-1799, USA*⁵*Department of Physics and Astronomy, University of South Carolina, Columbia, SC 29208, USA*

(Received 7 October 2009; published 22 March 2010)

We study coherent pion production in neutrino-nucleus scattering in the energy region relevant to neutrino oscillation experiments of current interest. Our approach is based on the combined use of the Sato-Lee model of electroweak pion production on a nucleon and the Δ -hole model of pion-nucleus reactions. Thus we develop a model that describes pion-nucleus scattering and electroweak coherent pion production in a unified manner. Numerical calculations are carried out for the case of the ^{12}C target. All the free parameters in our model are fixed by fitting to both total and elastic differential cross sections for π - ^{12}C scattering. Then we demonstrate the reliability of our approach by comparing our prediction for coherent pion photoproductions with the data. Finally, we calculate total and differential cross sections for neutrino-induced coherent pion production, and some of the results are compared with recent data from K2K, SciBooNE, and MiniBooNE. We also study the effect of nonlocality of Δ propagation in the nucleus and compare the elementary amplitudes used in different microscopic calculations.

DOI: [10.1103/PhysRevC.81.035502](https://doi.org/10.1103/PhysRevC.81.035502)

PACS number(s): 13.15.+g, 14.60.Pq, 25.30.Pt

I. INTRODUCTION

The detailed theoretical study of neutrino-nucleus reactions is of great current importance owing to the ever-increasing precision of neutrino oscillation experiments (recently carried out, ongoing, and forthcoming). Because most of these experiments measure the neutrino flux through neutrino-nucleus scattering, reliable theoretical estimates of the relevant cross sections are prerequisite for the accurate interpretation of the data. Some of these experiments (T2K, MiniBooNE, etc.) use neutrinos in an energy range within which the dominant processes are quasielastic nucleon knockout and quasifree single-pion production through excitation of the Δ (1232) resonance. Meanwhile, coherent single-pion production in this energy region (albeit not a dominant process) is also of considerable interest, as it allows us to study, with no ambiguity concerning the final nuclear state, the details of the Δ -excitation mechanism and medium effects on the pion; knowledge of these details is essential for predicting the dominant quasifree pion production processes. In this paper we focus on the coherent single-pion production process.

There have indeed been quite active experimental efforts to investigate neutrino-induced coherent single-pion production in the Δ -excitation region. K2K [1] and SciBooNE [2] investigated charged-current (CC) coherent pion production, while MiniBooNE [3] studied neutral-current (NC) coherent pion production. Furthermore, results for antineutrino-induced coherent pion-production processes are expected to become

available soon from MiniBooNE for the NC process [4] and from SciBooNE for the CC process [5]. It is to be remarked, however, that the recent experimental results offer a rather puzzling situation. The experiments at K2K [1] and SciBooNE [2] report that the CC process is not observed, whereas the MiniBooNE experiment [3] concludes that the NC process is observed. Now, from the isospin factors, we expect an approximate relation $\sigma_{CC} \sim 2\sigma_{NC}$. Although the muon mass can reduce the phase space for the CC process at low energies, we still expect that σ_{CC} should be of a significant size compared with σ_{NC} , and hence the above experimental results seem quite puzzling. In this connection it is to be noted that MiniBooNE's use of the Rein-Sehgal (RS) model [6] in analyzing the NC data has recently been questioned [7]: for a critical review of the RS model, see Refs. [7] and [8]. The CC data analyses in Refs. [1] and [2] did not rely on a particular theoretical model for coherent pion production itself, but in dealing with some other neutrino-nucleus reactions that entered into the analyses, certain models whose reliability was open to debate had to be invoked.

The theoretical treatment of coherent pion production can be categorized into two types: a partially conserved axial current (PCAC)-based model and a microscopic model. In the former approach, the hadronic matrix element for neutrino-induced pion production is related to the pion-nucleus (or pion-nucleon) scattering amplitude through the PCAC relation. Meanwhile, in the microscopic approach, the hadronic matrix element is calculated by summing the elementary amplitude for weak pion production off a single nucleon embedded in a nuclear environment.

A prominent example of the PCAC-based approach is the model due to Rein and Sehgal (RS model) [6] (cf. Ref. [9]). Because of its success in the high-energy neutrino process [10] ($E_\nu \gtrsim 2$ GeV, where E_ν is the incident neutrino energy) and

*satoshi@jlab.org; Current affiliation: Excited Baryon Analysis Center (EBAC), Thomas Jefferson National Accelerator Facility, Newport News, Virginia 23606, USA.

its simplicity, the RS model has been extensively used in analyzing data in neutrino-oscillation experiments. Several authors, however, have recently pointed out that the RS model does not give a reasonable description for relatively low-energy neutrino processes ($E_\nu \lesssim 2$ GeV) [7,8] and that the use of the RS model may have led to the puzzling experimental situation currently facing us. There have been several proposals [8,11–13] to remedy some of the possible insufficiencies in the original RS model.

Meanwhile, to build a quantitatively reliable microscopic approach, it is obviously of primary importance to start with a model that can describe with sufficient accuracy electroweak pion production off a free single nucleon. Furthermore, for pion production off a nuclear target, we need to consider medium effects such as the final-state interactions (FSIs) between the outgoing pion and nucleus, etc. Recently there have been several microscopic calculations [7,14–16], the most elaborate one being that by Amaro *et al.* [7]. These calculations differ in the way the elementary process ($\nu_\mu N \rightarrow \mu^+ N \pi$) is modeled and/or in the way the medium effects are taken into account. For example, only the resonant Δ -excitation mechanism is considered in Refs. [14] and [15], while the nonresonant mechanism is additionally considered in Refs. [7] and [16]. It was shown in Refs. [7] and [16] that inclusion of the nonresonant mechanism leads to a reduction in the cross section by a factor of ~ 2 , even though both models are constructed in such a manner that the data for the elementary process are reproduced fairly well.¹ This result indicates the importance of modeling the elementary process with a sound and systematic approach that has been extensively tested by available data.

The purpose of the present article is to develop an alternative microscopic model for coherent pion production. An important ingredient of our formalism is a reliable dynamical model for the elementary process, and for that we employ the Sato-Lee (SL) model [17,18]. The SL model was first developed as a systematic framework for studying resonance properties by analyzing data on pion production in photon (electron)-nucleon scattering in the Δ -resonance region [17,19]. The SL model treats the resonant and nonresonant mechanisms on the same footing and is known to provide a reasonably accurate description of an extensive set of pion production data. The SL model was further extended to the weak sector in Ref. [18] and was shown to be able to reproduce data for neutrino-induced pion production off a nucleon. As has been done in previous microscopic calculations, we also need to incorporate the nuclear medium effects. In the energy region of our interest, the Δ -hole approach has proved to be successful in describing various processes involving pion-nucleus dynamics. These situations motivate us to develop a model for coherent pion production by combining the SL model and the Δ -hole model, and this is what we attempt in this article. We limit ourselves here to a case where the target nucleus (and hence the final nucleus also) has spin 0 and employ a simplified Δ -hole model proposed in Ref. [20]. As

for concrete numerical calculations, we concentrate on the ^{12}C target, which has been and will continue to be an important nuclear target in many of neutrino-oscillation experiments. To test the reliability of our approach, we first calculate observables for coherent photopion production on ^{12}C using the same theoretical framework and show that the calculated results agree well with data. We then proceed to calculate observables for coherent neutrino-pion production on ^{12}C and present numerical results that can be compared with the recent data from K2K and SciBooNE. We also present theoretical predictions for those quantities for which experimental data will soon become available.

The fact that the previous microscopic calculations exhibit a rather large model dependence makes it particularly interesting to use the SL model, which has been highly successful in the single-nucleon sector. The SL model provides a consistent set of amplitudes for pion production and pion-nucleon scattering on a single nucleon; all these amplitudes are obtained in a systematic manner from the same Lagrangian. In our approach this consistency can be further taken over to the description of the FSI between the final pion and the nucleus. Thus, based on the SL amplitudes, we can construct a pion-nucleus optical potential that is consistent with the transition operators for electroweak pion production off a nucleus. To the best of our knowledge, our approach is the first to provide a consistent framework for treating the medium effect on the pion and electroweak pion production on the same footing. This point is worth emphasizing because it is this consistency that enables us to *predict* cross sections for electroweak coherent pion production *with no adjustable parameters*, once we fix certain parameters (see the following) relevant to medium effects by fitting to the pion-nucleus scattering data.

Another point to be noted is that our model takes into account the nonlocal effect for in-medium Δ propagation. For neutrino-induced coherent pion production, neither the RS-based nor previous microscopic models have included this effect. As pointed out in Ref. [21], the nonlocal effect could reduce the cross section by a factor of ~ 2 (~ 1.7) for $E_\nu = 0.5$ (1) GeV. We consider it important to take due account of the possibly large nonlocal effect.

Our calculation adopts the following procedure. We first construct a pion-nucleus optical potential, using the SL πN scattering (on- and off-shell) amplitudes as basic ingredient. The medium modification of the Δ propagation in a nucleus is considered with the use of the Δ -hole model [20]. All free parameters in our model (spreading potential, phenomenological terms in the optical potential) are fixed by fitting to pion-nucleus scattering data. After these parameters are determined, we are in a position to make a prediction of the coherent pion production process. Before calculating the neutrino-induced process, we test the reliability of our model by comparing our predictions for the photo-induced process with data. After finding satisfactory results for the photoprocess, we proceed to calculate neutrino-induced coherent pion production.

The organization of this paper is as follows. Section II is dedicated to the explanation of our approach. We first introduce the elementary amplitudes of the SL model. We then give expressions for calculating the electroweak coherent

¹Unfortunately, conclusive data for the elementary neutrino process are still lacking, which leads to theoretical uncertainty.

pion production amplitudes in terms of the SL amplitudes and derive the cross-section formulas. The expression for the constructed optical potential and its relation with the scattering amplitude are also given there. We present numerical results in Sec. III and give a conclusion in Sec. IV. Appendix A provides definitions of the multipole amplitudes, while Appendix B explains the Lorentz transformation used in our calculation. In Appendix C we give expressions for quantities that appear in the Δ -hole model.

II. FORMULATION

The kinematics of the reactions under consideration is as follows. We consider coherent pion production in neutrino(ν_ℓ)-nucleus(t) scattering: $\nu_\ell(p_\nu) + t(p_t) \rightarrow \ell^-(p'_\ell) + \pi^+(k) + t(p'_t)$ for the CC process, and $\nu_\ell(p_\nu) + t(p_t) \rightarrow \nu_\ell(p'_\ell) + \pi^0(k) + t(p'_t)$ for the NC process; we also consider the antineutrino counterparts. The four-momentum for each particle in the laboratory frame (LAB) is given in parentheses. The four-momentum transfer from the leptons is denoted $q^\mu \equiv p_\nu^\mu - p'_\ell{}^\mu$. We choose a right-handed coordinate system in which the z axis lies along the incident neutrino momentum \mathbf{p}_ν , and the y axis is taken along $\mathbf{p}_\nu \times \mathbf{p}'_\ell$. In evaluating a nuclear matrix element, it is convenient to work in the pion-nucleus center-of-mass frame (ACM). The kinematical variables in ACM are denoted by \mathbf{q}_A , \mathbf{k}_A , etc. We also work in the pion-nucleon center-of-mass frame (2CM), when calculating the elementary SL amplitudes. The kinematical variables in 2CM are denoted \mathbf{q}_2 , \mathbf{k}_2 , etc. When working in ACM (2CM), we choose a coordinate system in which the z axis lies along \mathbf{q}_A (\mathbf{q}_2) and the y axis is along $\mathbf{p}_{\nu,A} \times \mathbf{p}'_{\ell,A}$ ($\mathbf{p}_{\nu,2} \times \mathbf{p}'_{\ell,2}$).

A. The Sato-Lee model

We express nuclear transition amplitudes for coherent pion production in terms of the elementary amplitudes derived from the SL model [18]. In this section, therefore, we introduce the SL amplitudes. The differential cross section in the LAB frame for pion production in the neutrino-nucleon CC reaction, $\nu_\ell(p_\nu) + N(p_N) \rightarrow \ell^-(p'_\ell) + \pi^+(k) + N(p'_N)$, is given by [cf. Eq. (10) in Ref. [18]]

$$\frac{d^5\sigma}{dE'_\ell d\Omega'_\ell d\Omega_\pi} = \frac{G_F^2 \cos^2 \theta_c}{2} \left(\frac{|\mathbf{k}|}{\omega_\pi} + \frac{|\mathbf{k}| - \hat{\mathbf{k}} \cdot (\mathbf{p}_\nu - \mathbf{p}'_\ell)}{E'_N} \right)^{-1} \times \frac{|\mathbf{p}'_\ell| |\mathbf{k}|^2 m_N^2}{|\mathbf{p}_\nu| \omega_\pi E_N E'_N} \frac{L^{\mu\nu} W_{\mu\nu}}{(2\pi)^5}, \quad (1)$$

where $G_F = 1.16637 \times 10^{-5} \text{ GeV}^{-2}$ is the Fermi constant, and θ_c is the Cabbibo angle ($\cos \theta_c = 0.974$). E'_ℓ and ω_π are the energies of the final lepton and pion, respectively, m_N is the nucleon mass, and E_N (E'_N) is the initial (final) nucleon energy. $W_{\mu\nu}$ and $L^{\mu\nu}$ represent the hadron and the lepton tensors, respectively, and their definitions are given in Ref. [18] [Eqs. (11) and (12) therein]. The preceding cross section can

be written as

$$\frac{d^5\sigma}{dE'_\ell d\Omega'_\ell d\Omega_\pi} = \frac{G_F^2 \cos^2 \theta_c}{2} \left(\frac{|\mathbf{k}|}{\omega_\pi} + \frac{|\mathbf{k}| - \hat{\mathbf{k}} \cdot (\mathbf{p}_\nu - \mathbf{p}'_\ell)}{E'_N} \right)^{-1} \times \frac{|\mathbf{p}'_\ell| |\mathbf{k}|^2}{(2\pi)^5 |\mathbf{p}_\nu|} E'_{\ell,2} p_{\nu,2} \times \frac{1}{2} \sum_{s_N s'_N} \sum_{s'_\ell} |\Gamma_{2L}(F^V - F^A)|^2, \quad (2)$$

where F^V and F^A are the transition amplitudes in which the hadronic vector and the axial-vector currents are, respectively, contracted with the leptonic current. The symbol s_N (s'_N) is the z component of the initial (final) nucleon spin, while s'_ℓ denotes the final lepton spin. The energies of the final lepton and the initial neutrino in 2CM are denoted $E'_{\ell,2}$ and $p_{\nu,2}$, respectively. F^V and F^A , including both hadronic and lepton currents, are calculated in 2CM and then embedded in the cross-section expression given in LAB. The factor Γ_{2L} arises from the relevant Lorentz transformation (see Appendix B):

$$\Gamma_{2L} = \sqrt{\frac{\omega_{\pi,2} E_{N,2} E'_{N,2}}{\omega_\pi E_N E'_N}}, \quad (3)$$

where $\omega_{\pi,2}$, $E_{N,2}$, and $E'_{N,2}$ are the energies of the pion, the incident nucleon, and the final nucleon in 2CM. The spin structure of F^V and F^A can be parametrized as

$$\begin{aligned} F^V = & -i\vec{\sigma} \cdot \vec{\epsilon}_\perp F_1^V - \vec{\sigma} \cdot \hat{\mathbf{k}}_2 \vec{\sigma} \cdot \hat{\mathbf{q}}_2 \times \vec{\epsilon}_\perp F_2^V \\ & - i\vec{\sigma} \cdot \hat{\mathbf{q}}_2 \hat{\mathbf{k}}_2 \cdot \vec{\epsilon}_\perp F_3^V - i\vec{\sigma} \cdot \hat{\mathbf{k}}_2 \hat{\mathbf{k}}_2 \cdot \vec{\epsilon}_\perp F_4^V \\ & - i\vec{\sigma} \cdot \hat{\mathbf{q}}_2 \hat{\mathbf{q}}_2 \cdot \vec{\epsilon} F_5^V - i\vec{\sigma} \cdot \hat{\mathbf{k}}_2 \hat{\mathbf{q}}_2 \cdot \vec{\epsilon} F_6^V \\ & + i\vec{\sigma} \cdot \hat{\mathbf{k}}_2 \epsilon_0 F_7^V + i\vec{\sigma} \cdot \hat{\mathbf{q}}_2 \epsilon_0 F_8^V, \end{aligned} \quad (4)$$

where $\vec{\epsilon}_\perp = \hat{\mathbf{q}}_2 \times (\vec{\epsilon} \times \hat{\mathbf{q}}_2)$ and

$$\begin{aligned} F^A = & -i\vec{\sigma} \cdot \hat{\mathbf{k}}_2 \vec{\sigma} \cdot \vec{\epsilon}_\perp F_1^A - \vec{\sigma} \cdot \hat{\mathbf{q}}_2 \times \vec{\epsilon}_\perp F_2^A \\ & - i\vec{\sigma} \cdot \hat{\mathbf{k}}_2 \vec{\sigma} \cdot \hat{\mathbf{q}}_2 \hat{\mathbf{k}}_2 \cdot \vec{\epsilon}_\perp F_3^A - i\hat{\mathbf{k}}_2 \cdot \vec{\epsilon}_\perp F_4^A \\ & - i\vec{\sigma} \cdot \hat{\mathbf{k}}_2 \vec{\sigma} \cdot \hat{\mathbf{q}}_2 \hat{\mathbf{q}}_2 \cdot \vec{\epsilon} F_5^A - i\hat{\mathbf{q}}_2 \cdot \vec{\epsilon} F_6^A \\ & + i\epsilon_0 F_7^A + i\vec{\sigma} \cdot \hat{\mathbf{k}}_2 \vec{\sigma} \cdot \hat{\mathbf{q}}_2 \epsilon_0 F_8^A. \end{aligned} \quad (5)$$

The lepton-current matrix element ϵ^μ is given by $\epsilon^\mu = \langle \ell | \bar{\psi}_l \gamma^\mu (1 - \gamma_5) \psi_\nu | \nu_\ell \rangle$. We have introduced parametrization for F^A simply via $F^A = \vec{\sigma} \cdot \hat{\mathbf{k}}_2 F^V$. The amplitudes, F_i^V and F_i^A , are expressed in terms of the multipole amplitudes $E_{l\pm}^{V,A}$, $M_{l\pm}^{V,A}$, $S_{l\pm}^{V,A}$, and $L_{l\pm}^A$, which are functions of q^2 and W (the πN invariant mass) and computed in 2CM. Their explicit expressions are presented in Appendix A.

In a coherent process on a spin-0 target under consideration, only the spin nonflip terms of the transition amplitudes contribute. We therefore can work with $\bar{F}^{V(A)}$, defined by

$$\bar{F}^{V(A)} = \frac{1}{2} \text{Tr}[F^{V(A)}], \quad (6)$$

where the trace is taken for nucleon spin space. Their explicit forms are

$$\bar{F}^V = -\hat{\mathbf{k}}_2 \cdot \hat{\mathbf{q}}_2 \times \vec{\epsilon}_\perp F_2^V \quad (7)$$

and

$$\begin{aligned}\bar{F}^A = & -i\hat{k}_2 \cdot \bar{\epsilon}_\perp F_1^A - i\hat{k}_2 \cdot \hat{q}_2 \hat{k}_2 \cdot \bar{\epsilon}_\perp F_3^A - i\hat{k}_2 \cdot \bar{\epsilon}_\perp F_4^A \\ & - i\hat{k}_2 \cdot \hat{q}_2 \hat{q}_2 \cdot \bar{\epsilon} F_5^A - i\hat{q}_2 \cdot \bar{\epsilon} F_6^A + i\epsilon_0 F_7^A + i\hat{k}_2 \cdot \hat{q}_2 \epsilon_0 F_8^A.\end{aligned}\quad (8)$$

In particular, the resonant parts of the elementary amplitudes are given by

$$\begin{aligned}\bar{F}_R^V - \bar{F}_R^A = & (-2\hat{k}_2 \cdot \hat{q}_2 \times \bar{\epsilon}_\perp M_{R1+}^{(3/2),V} - 2i\hat{k}_2 \cdot \bar{\epsilon}_\perp E_{R1+}^{(3/2),A} \\ & - 4i\hat{k}_2 \cdot \hat{q}_2 \epsilon_0 S_{R1+}^{(3/2),A} + 4i\hat{k}_2 \cdot \hat{q}_2 \hat{q}_2 \cdot \bar{\epsilon} L_{R1+}^{(3/2),A}) \Lambda_{ij}^{3/2},\end{aligned}\quad (9)$$

where the subscript R stands for the resonant parts of the corresponding multipole amplitudes associated with the excitation of the Δ resonance. From the resonant amplitude we can factor out the Δ propagator $D(W)$ as

$$\bar{F}_R^V - \bar{F}_R^A = \frac{N(k_2, q_2)}{D(W)}, \quad (10)$$

and

$$D(W) = W - m_\Delta - \Sigma_\Delta(W), \quad (11)$$

where m_Δ and Σ_Δ are the bare mass and self-energy of the Δ resonance, respectively.

We next discuss the T -matrix element for πN scattering, which serves as an input for constructing an optical potential for pion-nucleus scattering. A calculational procedure for the πN T matrix within the SL model is given in Ref. [17]. A distorted wave obtained with this optical potential will be used to take account of the final-state interaction in coherent pion production. The T matrix is decomposed into the resonant (t_R) and nonresonant (t_{nr}) parts as

$$t_{\pi N}^{(c)} = t_R^{(c)} + t_{nr}^{(c)}, \quad (12)$$

where the superscript (c) specifies a channel; in our model the resonance amplitude exists only for the P_{33} channel. The on-shell component of the T matrix given in Eq. (12) is related to the phase shift by

$$t_{\pi N}^{(c)} = -\frac{W}{\pi \omega_{\pi,2} E_{N,2}} \frac{e^{2i\delta^{(c)}} - 1}{2ik_2^o}, \quad (13)$$

where W is the invariant mass of the πN system, and $\omega_{\pi,2} = \sqrt{k_2^{o2} + m_\pi^2}$ and $E_{N,2} = \sqrt{k_2^{o2} + m_N^2}$ are the on-shell energies of the pion and the nucleon in 2CM, respectively. The resonant amplitude is expressed as

$$t_R^{(P_{33})}(k_2', k_2; W) = -\frac{F_{\pi N \Delta}(k_2') F_{\pi N \Delta}(k_2)}{D(W)}, \quad (14)$$

where $F_{\pi N \Delta}(k_2)$ is the dressed $\pi N \Delta$ vertex, and $D(W)$ is the Δ propagator introduced in Eq. (11). We note that the four-momenta, k_2 and k_2' , are in general off energy shell.

B. Coherent pion production in neutrino-nucleus scattering

Similarly to Eq. (12) for the πN scattering amplitude, the weak amplitudes $\bar{F}^{V(A)}$, defined in Eqs. (6)–(8), also have

a resonant $\bar{F}_R^{V(A)}$ and a nonresonant $\bar{F}_{nr}^{V(A)}$ part. Accordingly, the transition amplitudes of coherent pion production on nuclei have resonant and nonresonant parts. We now describe how these two components are calculated in our approach.

1. Transition matrix element: resonant part

The main task in calculating the resonant part of coherent pion production on nuclei is to account for the medium effects on Δ propagation in the elementary resonant amplitudes $F_R^{V(A)}$. Here we follow the procedure of the Δ -hole model of pion-nucleus reactions by modifying the Δ propagator in Eq. (11). Thus it is useful to first briefly explain how the Δ -hole model is formulated by considering elastic pion-nucleus scattering; for a full account of the formulation see Refs. [22–25].

The Δ -hole model is formulated within the projection operator formalism [22]. The nuclear Fock space is divided into four spaces: P_0 , P_1 , D , and Q . The P_0 space is spanned by the pion and the nuclear ground state, the P_1 space by the pion and one-particle one-hole states, the D space by the one- Δ one-hole configurations, and $Q = 1 - P_0 - P_1 - D$ contains the remainder of the full space. A projected Hamiltonian is written as, for example, $H_{P_0 D} = P_0 H D$. Starting with the Schrödinger equation in the full space ($H|\Psi\rangle = E|\Psi\rangle$), we can apply the standard projection operator techniques [22] to obtain an equation, defined only in the P_0 space, to describe the pion-nucleus elastic scattering T matrix. In the Δ -hole model, one further imposes the condition that the D space is the doorway of the transitions between $P = P_0 + P_1$ and Q spaces; namely, $H_{PQ} = H_{QP} = 0$. The pion-nucleus scattering amplitude owing to Δ excitation can then be written as

$$T_{P_0 P_0}(E) = H_{P_0 D} G_{\Delta h}(E) H_{D P_0}, \quad (15)$$

where the total energy defined in ACM ($E + Am_N$) is given by

$$\begin{aligned}E + Am_N = & q_A^0 + \sqrt{q_A^2 + (Am_N)^2} \\ = & \sqrt{k_A^2 + m_\pi^2} + \sqrt{k_A^2 + (Am_N)^2},\end{aligned}\quad (16)$$

where A is the mass number. The Δ -hole propagator $G_{\Delta h}$ in Eq. (15) is defined by

$$G_{\Delta h}^{-1} = D(E - H_\Delta) - W_{el} - \Sigma_{\text{pauli}} - \Sigma_{\text{spr}}. \quad (17)$$

Here $D(E - H_\Delta)$ can be calculated from Eq. (11), with H_Δ being the Hamiltonian for the Δ particle in the nuclear many-body system. The effects owing to the Q space are included in the so-called spreading potential Σ_{spr} . A microscopic calculation of the spreading potential is very complicated, as it involves the calculation of pion absorption by two or more nucleons. It is therefore a common practice to determine Σ_{spr} phenomenologically by fitting to the pion-nucleus scattering data. Excitations to the P_1 space are included in the Δ self-energy $\Sigma_\Delta(W)$ of $D(E - H_\Delta)$ [see Eq. (11)] with a correction owing to Pauli blocking (Σ_{pauli}). De-excitation to the P_0 space is the rescattering in the elastic mode and is denoted W_{el} . In our actual calculation, we expand $G_{\Delta h}$ in term

of W_{el} , and the expansion series is resummed by solving the Lippmann-Schwinger (LS) equation.

The calculations of the pion-nucleus scattering amplitude in Eq. (15) require a diagonalization of the Δ -hole propagator $G_{\Delta h}$ of Eq. (17). For the diagonalization, it is practically convenient to work with the oscillator basis for the Δ state, defined by the Hamiltonian H_{Δ} , and the nucleon-hole state. This diagonalization is a difficult numerical task. Although an efficient method using the doorway-state expansion has been developed [24], the diagonalization of $G_{\Delta h}$ is still difficult, particularly for heavier nuclei. In Ref. [20], Karaoglu and Moniz (KM) proposed a simplified calculation with the Δ -hole model in which $G_{\Delta h}$ is calculated with a local density approximation rather than a diagonalization. In their simplified treatment, Σ_{pauli} is calculated by a nuclear matter calculation [26], and their result is given in Appendix C. Their parametrization of the spreading potential Σ_{spr} in terms of a central and a spin-orbit term is also given in Appendix C. Each term of the spreading potential has a complex strength, which is determined by fitting to the pion-nucleus scattering data. KM applied their approach to π - ^{16}O scattering and found a good agreement between their calculation and the data and, also, the full Δ -hole calculation [23,24] except for the most central partial waves. Encouraged by this success, we follow this simplified version of the Δ -hole model to include the medium effects on Δ propagation in defining the electroweak pion production matrix elements.

Schematically, the resonant part of the transition matrix element \mathcal{M}_R^A of weak coherent pion production on nuclei induced by the CC can be obtained by replacing the initial $H_{D P_0}$ in Eq. (15) with $H_{D P'_0}$ where P'_0 is the space spanned by the (axial-)vector current and the nucleus in the ground state. In terms of the single-particle wave functions $\psi_j(\mathbf{p}_N)$ of the nucleons in the initial and final nuclear states, we thus have²

$$\begin{aligned} \mathcal{M}_R^A &= \sum_j \int \frac{d^3 p_N}{(2\pi)^3} \frac{d^3 p'_N}{(2\pi)^3} \psi_j^*(\mathbf{p}'_N) \\ &\times \frac{\Gamma_{2A} N(k_2, q_2) (2\pi)^3 \delta(\mathbf{p}_N + \mathbf{q}_A - \mathbf{p}'_N - \mathbf{k}_A)}{D(E + m_N - H_{\Delta}) - \Sigma_{\text{pauli}} - \Sigma_{\text{spr}}} \psi_j(\mathbf{p}_N) \\ &= \sum_j \int \frac{d^3 p_{\Delta}}{(2\pi)^3} \psi_j^*(\mathbf{p}'_N) \\ &\times \frac{\Gamma_{2A} N(k_2, q_2)}{D(E + m_N - H_{\Delta}) - \Sigma_{\text{pauli}} - \Sigma_{\text{spr}}} \psi_j(\mathbf{p}_N), \end{aligned} \quad (18)$$

where $\mathbf{p}_{\Delta} = \mathbf{p}_N + \mathbf{q}_A = \mathbf{p}'_N + \mathbf{k}_A$; the index j denotes single-particle quantum numbers including the isospin. The summation (\sum_j) is taken over the occupied states of the nucleus. The factor Γ_{2A} is defined by

$$\Gamma_{2A} = \sqrt{\frac{\omega_{\pi,2} E_{N,2} E'_{N,2}}{\omega_{\pi,A} E_{N,A} E'_{N,A}}}, \quad (19)$$

where ω_{π} , E_N , and E'_N are the energies of the pion, the incoming nucleon, and the outgoing nucleon, respectively, and

²In Ref. [27], the authors carried out a calculation for photon-induced coherent pion production by diagonalizing $G_{\Delta h}$.

the quantities in the numerator (denominator) refer to 2CM (ACM). This factor arises from the fact that $\bar{F}_R^{V(A)}$ values computed in 2CM are to be embedded in \mathcal{M}_R^A evaluated in ACM. To evaluate the numerator in the integrand of Eq. (18), we clearly need a prescription for relating variables in 2CM to those in ACM. Here we use the commonly used prescription [28,29] to fix the nucleon momenta with the lepton momentum transfer \mathbf{q}_A and outgoing pion momentum \mathbf{k}_A as

$$\begin{aligned} \mathbf{p}_N &= -\frac{\mathbf{q}_A}{A} - \frac{A-1}{2A}(\mathbf{q}_A - \mathbf{k}_A), \\ \mathbf{p}'_N &= -\frac{\mathbf{k}_A}{A} + \frac{A-1}{2A}(\mathbf{q}_A - \mathbf{k}_A), \end{aligned} \quad (20)$$

and write the πN invariant mass as

$$W = \sqrt{(E_{NA} + q_A^0)^2 - (\mathbf{p}_N + \mathbf{q}_A)^2}, \quad (21)$$

with $E_{NA} = \sqrt{\mathbf{p}_N^2 + m_N^2}$. Having specified all the relevant variables in ACM, we can derive the corresponding variables in 2CM via a Lorentz transformation to obtain $N(k_2, q_2)$ of Eq. (18). For more details about this Lorentz transformation (including the discussion of a somewhat different treatment of an off-shell pion momentum), see Appendix B. Note that, in treating the wave functions, $\psi(\mathbf{p}_N)$ and $\psi(\mathbf{p}'_N)$, and the Δ kinetic term in the denominator in the integrand of Eq. (18), we do *not* use the prescription given in Eqs. (20) and (21); thus the important recoil effects on Δ propagation are not neglected in our calculations.

We incorporate the recoil effect on the Δ self-energy in the first-order approximation. This is done by linearizing the Δ propagator with the following expansion [25]:

$$D(E + m_N - H_{\Delta}) \sim D(W) - \gamma(W)(H_{\Delta} - e_{\Delta}^0), \quad (22)$$

$$E + m_N = W + e_{\Delta}^0, \quad (23)$$

$$\gamma(W) = \partial D(W)/\partial W, \quad (24)$$

$$H_{\Delta} = \frac{\mathbf{p}_{\Delta}^2}{2\mu_{\Delta}} + V_{\Delta} + V_{\Delta}^C + e_N, \quad (25)$$

$$1/\mu_{\Delta} = 1/m_{\Delta} + 1/(A-1)m_N, \quad (26)$$

where V_{Δ} (V_{Δ}^C) is the Δ (Coulomb) potential in the nucleus, and e_N is the hole energy. The Δ potential is taken to be the same as that for the nucleon; its explicit expression is given in Appendix C. Equation (23) defines e_{Δ}^0 . To carry out the integration over the Δ momentum \mathbf{p}_{Δ} in Eq. (18), we express the nucleon wave function $\psi_j(\mathbf{p})$ in terms of its coordinate-space form $\phi_j(\mathbf{r})$. We note that with the prescription in Eqs. (20) and (21), the numerator $N(k_2, q_2)$ of Eq. (18) is independent of the variable \mathbf{p}_{Δ} and can be factorized out of the integration. With this factorization approximation and with the use of the linearized form in Eq. (22), the integration over \mathbf{p}_{Δ} leads to the following r -space expression:

$$\begin{aligned} \mathcal{M}_R^A &= -\left(\frac{\mu_{\Delta} \Gamma_{2A} N(k_2, q_2)}{2\pi \gamma}\right) \sum_j \int d^3 r d^3 r' \\ &\times \phi_j^*(\mathbf{r}') e^{-i\mathbf{k}_A \cdot \mathbf{r}'} \frac{e^{iK_{\Delta} |\mathbf{r}' - \mathbf{r}|}}{|\mathbf{r}' - \mathbf{r}|} e^{i\mathbf{q}_A \cdot \mathbf{r}} \phi_j(\mathbf{r}), \end{aligned} \quad (27)$$

where

$$K_{\Delta}^2 = \frac{2\mu_{\Delta}}{\gamma} \{W - m_{\Delta} - \Sigma_{\Delta}(W) + \gamma(E - W + m_N) - \gamma[e_N + V_{\Delta} + V_{\Delta}^C] - \Sigma_{\text{pauli}} - \Sigma_{\text{spr}}\}. \quad (28)$$

Following the procedure described in Ref. [20] [see Eqs. (25)–(39) therein], and subsequently applying the Lorentz transformation from ACM to LAB, we obtain the following expression for the transition matrix element \mathcal{M}_R^L in LAB:

$$\begin{aligned} \mathcal{M}_R^L &= \frac{16\sqrt{1+|\lambda|\pi}}{3} \frac{\mu_{\Delta} D(W)}{\gamma} \Gamma_{2L} \\ &\times (-2\hat{k}_2 \cdot \hat{q}_2 \times \vec{\epsilon}_{\perp} M_{R1+}^{(3/2),V} - 2i\hat{k}_2 \cdot \vec{\epsilon}_{\perp} E_{R1+}^{(3/2),A} \\ &- 4i\hat{k}_2 \cdot \hat{q}_2 \epsilon_0 S_{R1+}^{(3/2),A} + 4i\hat{k}_2 \cdot \hat{q}_2 \hat{q}_2 \cdot \vec{\epsilon} L_{R1+}^{(3/2),A}) \\ &\times \sum_{N=p,n} \left(1 + \frac{\lambda\tau_N}{2}\right) \int s^2 ds R^2 dR j_0(pR) j_0(PS) \frac{e^{i\bar{K}_{\Delta}s}}{s} \\ &\times \left\{1 + \frac{i\mu_{\Delta}s}{\bar{K}_{\Delta}} [\bar{e}_N + H_N]\right\} \rho_N(R) \hat{j}_1(k_F s), \quad (29) \end{aligned}$$

where $p = |\mathbf{k}_A - \mathbf{q}_A|$, $P = |\mathbf{k}_A + \mathbf{q}_A|/2$, $s = |\mathbf{r}' - \mathbf{r}|$, $R = |\mathbf{r}' + \mathbf{r}|/2$, and \bar{K}_{Δ} is obtained from K_{Δ} by replacing e_N with its average value, \bar{e}_N ; we choose $\bar{e}_N = 16$ MeV. The 2CM variables k_2 and q_2 are obtained from k_A and q_A using the Lorentz transformation as mentioned previously. The variable λ denotes the charge state of the outgoing pion, while $\tau_N = 1(-1)$ for $N = \text{proton (neutron)}$. The factor Γ_{2L} is from the Lorentz transformation from 2CM to LAB and is defined by

$$\Gamma_{2L} = \sqrt{\frac{\omega_{\pi,2} E_{N,2} E'_{N,2}}{\omega_{\pi,L} E_{N,L} E'_{N,L}}}. \quad (30)$$

In Eq. (29), $j_{\ell}(x)$ is the spherical Bessel function of order ℓ , and $\hat{j}_1(x) \equiv \frac{3}{x} j_1(x)$; k_F is the Fermi momentum,

$$k_F^3(R) = \frac{3\pi^2}{2} \rho_N(R). \quad (31)$$

The proton (neutron) matter density is denoted ρ_p (ρ_n) and is normalized to the total number of protons (neutrons) inside the target. For the proton matter form factor we use the empirical nuclear charge form factor [30] divided by the proton charge form factor [31]. The neutron matter density is assumed to be the same as the proton matter density.

The single-nucleon Hamiltonian appearing in Eq. (29) is given by

$$H_N = -\frac{\nabla_s^2}{2m_N} - \frac{\nabla_R^2}{8m_N} + V[(R^2 + s^2/4)^{1/2}], \quad (32)$$

where V is the single-particle potential [Eq. (C8)].

To take account of the final pion-nucleus interactions, we convolute the matrix element \mathcal{M}_R^L of Eq. (29) with the pion distorted wave, which is expanded in partial waves:

$$\chi_{\lambda}^*(\mathbf{k}'_A) = \sum_{l_{\pi} m_{\pi}} \chi_{\lambda, l_{\pi}}^*(k'_A) Y_{l_{\pi} m_{\pi}}^*(\hat{\mathbf{k}}_A) Y_{l_{\pi} m_{\pi}}(\hat{\mathbf{k}}'_A), \quad (33)$$

where k'_A is the off-shell momentum. We note that the pion distorted wave also depends on the pion charge (λ). More

details on our calculations of the pion wave functions are given in Sec. IID.

By performing the partial-wave decomposition of \mathcal{M}_R^L (now defined by the off-shell pion momentum by setting $\mathbf{k}_A \rightarrow \mathbf{k}'_A$) and using Eq. (33), the amplitude \mathcal{M}_R^L with pion-nucleus FSI takes the following form:

$$\begin{aligned} \mathcal{M}_R^L &= \epsilon_A^{\mu} \sum_{l_{\pi}} [P_{l_{\pi}}^1(x_A) (\cos \phi_A^{\pi} I_{E\mu}^{l_{\pi} 1} - i \sin \phi_A^{\pi} I_{M\mu}^{l_{\pi} 1}) \\ &+ P_{l_{\pi}}^1(x_A) (\sin \phi_A^{\pi} I_{E\mu}^{l_{\pi} 2} + i \cos \phi_A^{\pi} I_{M\mu}^{l_{\pi} 2}) \\ &- 2P_{l_{\pi}}(x_A) I_{L\mu}^{l_{\pi} 3} + 2P_{l_{\pi}}(x_A) I_{S\mu}^{l_{\pi} 0}], \quad (34) \end{aligned}$$

where $x_A = \hat{q}_A \cdot \hat{k}_A$, ϕ_A^{π} is the azimuthal angle of the pion, and ϵ_A^{μ} is the lepton-current matrix element in ACM. The associated Legendre function of degree l_{π} and order 0 (1) is denoted $P_{l_{\pi}} (P_{l_{\pi}}^1)$. We have introduced the quantities $I_{X\mu}^{l_{\pi} v}$, defined by

$$\begin{aligned} I_{X\mu}^{l_{\pi} v} &= -i \frac{32\sqrt{1+|\lambda|\pi}\mu_{\Delta}}{3} \int dk'_A k_A'^2 \chi_{\lambda, l_{\pi}}^*(k'_A) \\ &\times \int dx'_A \Lambda_{\mu}^v \Gamma_{AL}^{\lambda} \Gamma_{2AL} \gamma^{-1} X_R \xi_{l_{\pi}}^X(x'_A) \\ &\times \sum_{N=p,n} \left(1 + \frac{\lambda\tau_N}{2}\right) \int s^2 ds R^2 dR j_0(pR) j_0(PS) \frac{e^{i\bar{K}_{\Delta}s}}{s} \\ &\times \left\{1 + \frac{i\mu_{\Delta}s}{\bar{K}_{\Delta}} [\bar{e}_N + H_N]\right\} \rho_N(R) \hat{j}_1(k_F s), \quad (35) \end{aligned}$$

where $x'_A = \hat{q}_A \cdot \hat{k}'_A$, $x'_2 = \hat{q}_2 \cdot \hat{k}'_2$, and

$$\xi_{\ell l_{\pi}}^X(x'_A) = \begin{cases} \frac{2l_{\pi} + 1}{2l_{\pi}(l_{\pi} + 1)} P_{\ell}^1(x'_2) P_{l_{\pi}}^1(x'_A), & (X = E, M), \\ \frac{2l_{\pi} + 1}{2} P_{\ell}(x'_2) P_{l_{\pi}}(x'_A), & (X = L, S), \end{cases} \quad (36)$$

and

$$\frac{X_R}{D(W)} = E_{R1+}^{(3/2),A}, \quad M_{R1+}^{(3/2),V}, \quad L_{R1+}^{(3/2),A}, \quad S_{R1+}^{(3/2),A}, \quad (37)$$

for $X = E, M, L, S$.

The Lorentz transformation factors coming from the electroweak amplitudes (Γ_{2AL}) and the wave function (Γ^X) in Eq. (35) are, respectively,

$$\Gamma_{2AL} = \sqrt{\frac{\omega'_{\pi,2} E'_{N,2} E_{N,2}^i}{\omega'_{\pi,A} E'_{N,L} E_{N,L}^i}}, \quad \Gamma^X = \sqrt{\frac{\omega_{\pi,A} E_{N,A}'' E_{N,A}^f}{\omega_{\pi,L} E_{N,L}'' E_{N,L}^f}}, \quad (38)$$

where ω'_{π} is the pion energy in the intermediate state, E_N^i and E_N^f are the nucleon energies in the initial and final states, and E_N^i and E_N'' are those in the intermediate states; in general, E_N^i and E_N'' can be different. As before, the subscripts $\{2, A, L\}$ attached to the energies specify reference frames. It is noted that the multipole amplitudes (X_R^A) depend on x'_A because the πN invariant mass in the intermediate state depends on it [Eqs. (20) and (21)]. We also have introduced the Lorentz matrix Λ_{μ}^v defined by $\epsilon_2^v = \Lambda_{\mu}^v \epsilon_A^{\mu}$; Λ_{μ}^v also depends on x'_A ; the same Lorentz matrix relates $q_A (k'_A)$ to $q_2 (k'_2)$. A procedure

for deriving the Lorentz matrix and the transformation factors in Eq. (38) is explained in Appendix B.

2. Transition matrix element: nonresonant part

We assume that there is no medium effect on the nonresonant part, $\bar{F}_{\text{nr}}^V - \bar{F}_{\text{nr}}^A$, of the weak pion production amplitude on a nucleon in nuclei. Including the final pion-nucleus interactions and using the same factorization approximation, based on the choice [Eq. (20)] of the nucleon momenta to evaluate $\bar{F}_{\text{nr}}^V - \bar{F}_{\text{nr}}^A$, the nonresonant coherent pion production matrix element $\mathcal{M}_{\text{nr}}^L$ can be written as

$$\mathcal{M}_{\text{nr}}^L = \sum_{N=p,n} \int d^3k'_A \chi_{\lambda}^*(\mathbf{k}'_A) \times \Gamma_{AL}^X \Gamma_{2AL} F_N(\mathbf{k}'_A - \mathbf{q}_A) (\bar{F}_{\text{nr}}^{V,\zeta} - \bar{F}_{\text{nr}}^{A,\zeta}), \quad (39)$$

where $\bar{F}_{\text{nr}}^{V,\zeta}$ ($\bar{F}_{\text{nr}}^{A,\zeta}$) is the nonresonant part of \bar{F}^V (\bar{F}^A) given in Eqs. (7) and (8). $\bar{F}_{\text{nr}}^{V(A)}$ depends on N and λ [Eq. (A17)], and the set (N, λ) is collectively denoted ζ . The nuclear form factor $F_N(\mathbf{p})$ is given by

$$F_N(\mathbf{p}) = \int d^3r \rho_N(\mathbf{r}) e^{i\mathbf{p}\cdot\mathbf{r}}. \quad (40)$$

After the partial wave expansion of the pion distorted wave, we arrive at

$$\mathcal{M}_{\text{nr}}^L = \epsilon_A^\mu \sum_{l_\pi} [P_{l_\pi}^1(x_A) (\cos \phi_A^\pi J_{E\mu}^{l_\pi 1} - i \sin \phi_A^\pi J_{M\mu}^{l_\pi 1}) + P_{l_\pi}^1(x_A) (\sin \phi_A^\pi J_{E\mu}^{l_\pi 2} + i \cos \phi_A^\pi J_{M\mu}^{l_\pi 2}) - P_{l_\pi}^1(x_A) J_{L\mu}^{l_\pi 3} + P_{l_\pi}^1(x_A) J_{S\mu}^{l_\pi 0}], \quad (41)$$

where we have introduced $J_{X\mu}^{l_\pi v}$, defined by

$$J_{X\mu}^{l_\pi v} = -4\pi i \int dk'_A k_A'^2 \chi_{\lambda l_\pi}^*(k'_A) \int dx'_A \Lambda_\mu^v \Gamma_{AL}^X \Gamma_{2AL} \times \sum_{\ell} \xi_{\ell l_\pi}^X(x'_A) \sum_{N=p,n} X_{\text{nr}}^{\ell,\zeta} \int r^2 dr \rho_N(r) j_0(pr), \quad (42)$$

for $X = E, M, L, S$. The multipole amplitudes are included in $X_{\text{nr}}^{\ell,\zeta}$ as

$$X_{\text{nr}}^{\ell,\zeta} = (\ell + 1)^2 X_{\text{nr}\ell+}^{A,\zeta} + \ell^2 X_{\text{nr}\ell-}^{A,\zeta}, \quad (43)$$

for $X = L, S$, and

$$E_{\text{nr}}^{\ell,\zeta} = (\ell + 1) E_{\text{nr}\ell+}^{A,\zeta} - \ell E_{\text{nr}\ell-}^{A,\zeta}, \quad (44)$$

$$M_{\text{nr}}^{\ell,\zeta} = (\ell + 1) M_{\text{nr}\ell+}^{V,\zeta} + \ell M_{\text{nr}\ell-}^{V,\zeta}, \quad (45)$$

for $X = E, M$. The ζ dependence of the multipole amplitudes is indicated explicitly. For example, $E_{\text{nr}\ell+}^{A,\zeta}$ is the nonresonant part of $E_{\ell+}^A$, which has been introduced previously. The same rule applies to the other multipole amplitudes.

3. Cross section

Having written the transition amplitude for the coherent process in terms of the SL multipole amplitudes, we can proceed to calculate the cross section for the CC process. First,

we write the transition amplitudes in Eqs. (34) and (41) as

$$\mathcal{M}_R^L = \bar{\mathcal{M}}_{R,\mu}^L \epsilon_A^\mu, \\ \mathcal{M}_{\text{nr}}^L = \bar{\mathcal{M}}_{\text{nr},\mu}^L \epsilon_A^\mu.$$

In the LAB frame, the differential cross section for $\nu_\ell(p_\nu) + t(p_t) \rightarrow \ell^-(p'_\ell) + \pi^+(k) + t(p'_t)$ is then given by

$$\frac{d^5\sigma}{dE'_\ell d\Omega'_\ell d\Omega_\pi} = \frac{G_F^2 \cos^2 \theta_c}{2} \left(\frac{|\mathbf{k}|}{\omega_\pi} + \frac{|\mathbf{k}| - \hat{\mathbf{k}} \cdot (\mathbf{p}_\nu - \mathbf{p}'_\ell)}{E'_t} \right)^{-1} \times \frac{|\mathbf{p}'_\ell| |\mathbf{k}|^2}{(2\pi)^5 |\mathbf{p}_\nu|} E'_{\ell,A} p_{\nu,A} \times \sum_{s'_\ell} |(\bar{\mathcal{M}}_{R,\mu}^L + \bar{\mathcal{M}}_{\text{nr},\mu}^L) \epsilon_A^\mu|^2, \quad (46)$$

where $E'_t (= \sqrt{\mathbf{p}_t^2 + (Am_N)^2})$ is the total energy of the nucleus in the final state in LAB, and $E'_{\ell,A}$ and $p_{\nu,A}$ are the energies of the final lepton and the initial neutrino in ACM. Note that the calculation of $\sum_{s'_\ell} |(\bar{\mathcal{M}}_{R,\mu}^L + \bar{\mathcal{M}}_{\text{nr},\mu}^L) \epsilon_A^\mu|^2$ of Eq. (46) can make use of the following property:

$$L_A^{\mu\nu} \equiv \frac{E'_{\ell,A} p_{\nu,A}}{2} \sum_{s'_\ell} \epsilon_A^\mu \epsilon_A^{\nu*} = p_{\nu,A}^\mu p_{\ell,A}^{\nu'} + p_{\nu,A}^\nu p_{\ell,A}^{\mu'} - g^{\mu\nu} p_{\nu,A} \cdot p'_{\ell,A} \pm i \epsilon^{\mu\nu\rho\sigma} p_{\nu,A\rho} p'_{\ell,A\sigma}, \quad (47)$$

where $g^{\mu\nu}$ is the geometric tensor and $\epsilon^{\mu\nu\rho\sigma}$ is the antisymmetric tensor with $\epsilon^{0123} = 1$. The plus (minus) sign in the last term is for the (anti-) neutrino process.

To obtain the cross-section formula for the neutrino NC process, $\nu + t \rightarrow \nu + \pi^0 + t$, we make the following changes in Eq. (46). Remove the Cabbibo angle. Set the lepton mass equal to 0. Set the pion charge index λ (and ζ) to 0 in $I_{X\mu}^{l_\pi v}$ and $J_{X\mu}^{l_\pi v}$ ($X = E, M, L, S$) in Eqs. (35) and (42). [Note that the pion wave function ($\chi_{\lambda l_\pi}$) also contains λ dependence.] Finally, multiply the multipole amplitudes $M_{\ell+}^{(3,2,1/2),V}$ with $(1 - 2 \sin^2 \theta_W)$, where θ_W is the Weinberg angle ($\sin^2 \theta_W = 0.23$), and multiply $M_{\ell+}^{(0),V}$ with $(-2 \sin^2 \theta_W)$.

For the antineutrino CC process, the result for the neutrino CC process is modified as follows. Set the pion charge index λ (and ζ) to -1 in $I_{X\mu}^{l_\pi v}$ and $J_{X\mu}^{l_\pi v}$. Replace the lepton current by the one for the antineutrino process, which amounts to adopting the negative sign in the leptonic tensor, Eq. (47). The modifications needed for getting the cross section for the antineutrino NC process are now obvious.

C. Coherent pion photoproduction

With the same derivation given previously, we can also get an expression for the differential cross section of the coherent π^0 photoproduction process, $\gamma(q) + t(p_t) \rightarrow \pi^0(k) + t(p'_t)$, in the LAB frame:

$$\frac{d^2\sigma}{d\Omega_\pi} = \frac{\alpha}{2\pi} \left(\frac{|\mathbf{k}|}{\omega_\pi} + \frac{|\mathbf{k}| - \hat{\mathbf{k}} \cdot \mathbf{q}}{E'_t} \right)^{-1} \frac{|\mathbf{k}|^2}{|\mathbf{q}| \omega_\pi} \times \frac{1}{2} \sum_{\epsilon} |\mathcal{M}_R^\gamma + \mathcal{M}_{\text{nr}}^\gamma|^2, \quad (48)$$

where α is the fine structure constant, and $\frac{1}{2} \sum_{\epsilon}$ stands for averaging over the photon polarization. The transition amplitudes \mathcal{M}'_R and \mathcal{M}'_{nr} for the photoprocess are obtained from Eqs. (34) and (41) by retaining only the vector current, setting $\phi_A^\pi = 0$, and regarding ϵ_A^μ as the polarization vector of the incident photon. Finally, the pion charge index (λ) is set to 0 in $I_{X\mu}^{l\pi\nu}$ and $J_{X\mu}^{l\pi\nu}$ [Eqs. (35) and (42)].

D. Optical potential for pion-nucleus scattering

We calculate the pion-nucleus scattering using the computer code, PIPIT [32], by appropriately modifying the optical potential there to accommodate the dynamical features of the Δ -hole model and the SL model. In the original PIPIT, the optical potential (U), which is derived within the multiple scattering formalism by Kerman, McManus, and Thaler (KMT) [33], is given by³

$$U(\mathbf{k}'_A, \mathbf{k}_A) = \frac{A-1}{A} \{ \rho_p(\mathbf{q}) t_{\pi p}(\mathbf{k}'_A, \mathbf{k}_A; k_A^o) + \rho_n(\mathbf{q}) t_{\pi n}(\mathbf{k}'_A, \mathbf{k}_A; k_A^o) \}, \quad (49)$$

where \mathbf{k}_A (\mathbf{k}'_A) is the incoming (outgoing) pion momentum in ACM, and k_A^o the magnitude of the on-shell momentum. The quantity $\rho_p(\mathbf{q})$ ($\rho_n(\mathbf{q})$) is the form factor of the proton (neutron) matter distribution for $\mathbf{q} = \mathbf{k}_A - \mathbf{k}'_A$, and $t_{\pi p}$ ($t_{\pi n}$) is the pion-proton (pion-neutron) scattering T matrix whose normalization is defined in Eq. (13). It is to be noted that this original optical potential does not take account of Δ propagation in nuclei. In Ref. [20], KM separated $t_{\pi p}$ ($t_{\pi n}$) into the resonant and nonresonant parts, took the nonresonant and the Coulomb parts of the optical potential from the PIPIT code, and combined it with the resonant part derived from a simplified Δ -hole model. A phenomenological s -wave potential that is proportional to the square of the nuclear density ($\rho_t = \rho_p + \rho_n$) was also included to account for the pion absorption by two nucleons through non- Δ mechanisms. Thus the KM optical potential is given by

$$U(\mathbf{k}'_A, \mathbf{k}_A) = U_{nr} + U_R + U_{ph}(\rho_t^2), \quad (50)$$

where U_{nr} , U_R , and U_{ph} are the nonresonant, resonant, and phenomenological parts, respectively.

In constructing our optical potential, we follow the same separation as in Eq. (50). The nonresonant part of the optical potential is obtained from the PIPIT code by replacing the nonresonant T matrices in the original code with those derived from the SL model. It is worth emphasizing that the SL model provides both on-shell and off-shell T -matrix elements. Another difference from the original PIPIT code is that we use a different prescription for the Lorentz transformation from ACM to 2CM, as explained in Appendix B.

Regarding the resonant part, we use the resonant part of T matrix for the πN scattering from the SL model, basically following the procedure used in Ref. [20] [apart from a more elab-

orate treatment of kinematics (Lorentz transformation, etc.)]. First, we expand the optical potential into partial waves as

$$U(\mathbf{k}'_A, \mathbf{k}_A) = \frac{2}{\pi} \sum_{l_\pi m_\pi} V^{l_\pi}(k'_A, k_A) Y_{l_\pi m_\pi}^*(\hat{k}'_A) Y_{l_\pi m_\pi}(\hat{k}_A). \quad (51)$$

The resonant part of the potential is [cf. Eq. (39) of Ref. [20]]

$$\begin{aligned} V_R^{l_\pi}(k'_A, k_A) &= \frac{A-1}{A} \frac{8\pi^2 \mu_\Delta}{3} \\ &\times \int dx_A \Gamma_{A2} \gamma^{-1} x_2 P_{l_\pi}(x_A) F_{\pi N \Delta}(k'_2) F_{\pi N \Delta}(k_2) \\ &\times \sum_{N=p,n} \left(1 + \frac{\lambda \tau_N}{2} \right) \int s^2 ds R^2 dR j_0(pR) j_0(PS) \\ &\times \frac{e^{i\bar{K}_\Delta s}}{s} \left\{ 1 + \frac{i\mu_\Delta s}{\bar{K}_\Delta} [\bar{e}_N + H_N] \right\} \rho_N(R) \hat{j}_1(k_F s), \end{aligned} \quad (52)$$

where \mathbf{k}_2 (\mathbf{k}'_2) is the incoming (outgoing) pion momentum in 2CM, and $x_A = \hat{k}_A \cdot \hat{k}'_A$, $x_2 = \hat{k}_2 \cdot \hat{k}'_2$, $P = |\mathbf{k}_A + \mathbf{k}'_A|/2$, and $p = |\mathbf{k}_A - \mathbf{k}'_A|$. The dressed $\pi N \Delta$ coupling ($F_{\pi N \Delta}$) has been introduced in Eq. (14). The Lorentz transformation of the T matrix from 2CM to ACM gives rise to the factor Γ_{A2} defined by

$$\Gamma_{A2} = \sqrt{\frac{\omega_{\pi,2} \omega'_{\pi,2} E_{N,2} E'_{N,2}}{\omega_{\pi,A} \omega'_{\pi,A} E_{N,A} E'_{N,A}}}, \quad (53)$$

with $\omega_{\pi,2}^{(o)} = \sqrt{\mathbf{k}_2^{(o)2} + m_\pi^2}$, $\omega_{\pi,A}^{(o)} = \sqrt{\mathbf{k}_A^{(o)2} + m_\pi^2}$, $E_{N,2}^{(o)} = \sqrt{\mathbf{k}_2^{(o)2} + m_N^2}$, and $E_{N,A}^{(o)} = \sqrt{\mathbf{p}_{N,A}^{(o)2} + m_N^2}$. The values of $\mathbf{k}_2^{(o)}$ and $\mathbf{p}_{N,A}^{(o)}$ are fixed according to the prescription explained in Appendix B. The other quantities have been introduced in Sec. II B1.

Finally, we discuss the phenomenological term U_{ph} . We assume that in coordinate space U_{ph} can be parametrized as

$$U_{ph}(\mathbf{r}) = B \left(\frac{\rho_t(\mathbf{r})}{\rho_t(0)} \right)^2, \quad (54)$$

where B is the partial-wave-dependent strength of the potential. The corresponding partial-wave potential in momentum space is given by

$$\begin{aligned} V_{ph}^{l_\pi}(k'_A, k_A) &= \frac{A-1}{A} 4\pi^3 B_{l_\pi} \int_{-1}^1 dx_A P_{l_\pi}(x_A) \\ &\times \int dr r^2 j_0(pr) \left(\frac{\rho_t(r)}{\rho_t(0)} \right)^2. \end{aligned} \quad (55)$$

In the present calculation we include V_{ph}^0 and V_{ph}^1 and treat their strengths B_0 and B_1 as adjustable parameters. Thus our model contains as free parameters B_0 and B_1 (complex numbers) in addition to the couplings in the spreading potential.

Given the optical potential, we solve the LS equation,

$$\begin{aligned} T'_{l_\pi}(k'_A, k_A; k_A^o) &= V_{l_\pi}(k'_A, k_A; k_A^o) \\ &+ \frac{2}{\pi} \int \frac{V_{l_\pi}(k'_A, \bar{k}_A; k_A^o) T'_{l_\pi}(\bar{k}_A, k_A; k_A^o) \bar{k}_A^2 d\bar{k}_A}{\omega_\pi(k_A^o) + E_t(k_A^o) - \omega_\pi(\bar{k}_A) - E_t(\bar{k}_A) + i\epsilon}. \end{aligned} \quad (56)$$

³PIPIT also includes a finite-range Coulomb interaction, and corrections from the truncated part of the Coulomb interaction are taken into account using the Vincent-Phatak method [34].

The solution to this equation is used in two contexts. First, we use it to calculate the pion-nucleus elastic and total scattering cross sections and compare them with data to find the optimal values of the free parameters in our model. The solution to Eq. (56) is also used to compute the pion distorted-wave function that features in the matrix elements in Eqs. (35) and (42). For the former purpose, we obtain the full T matrix of pion-nucleus scattering from T' in Eq. (56) using the relation

$$T = \frac{A}{A-1} T'. \quad (57)$$

For charged-pion scattering, corrections for the finite-range Coulomb potential are incorporated with the use of the Vincent-Phatak method [34]. The procedure for calculating scattering observables from T is detailed in Ref. [32]. For the latter purpose, we calculate the pion distorted wave $\chi_{l_\pi}^*(k_A)$ associated with T' using the relation

$$\begin{aligned} \chi_{l_\pi}^*(k_A) = & \frac{\delta(k_A - k_A^o)}{k_A^2} \\ & + \frac{T'_{l_\pi}(k_A^o, k_A; k_A^o)}{\omega_\pi(k_A^o) + E_t(k_A^o) - \omega_\pi(k_A) - E_t(k_A) + i\epsilon}, \end{aligned} \quad (58)$$

where, for notational simplicity, dependence on the pion charge (λ) is suppressed. Following the KMT formalism [33], we use $\chi_{l_\pi}^*(k_A)$ in evaluating the matrix elements in Eqs. (35) and (42). This wave function is related to the full wave function by

$$\chi_{l_\pi}^{(\text{full})*} = -\frac{1}{A-1} + \frac{A}{A-1} \chi_{l_\pi}^*. \quad (59)$$

For charged-pion scattering, $\chi_{l_\pi}^{(\text{full})*}$ does not have the correct normalization, because the Coulomb potential has been cut off at a finite distance; this entails the necessity of multiplying $\chi_{l_\pi}^{(\text{full})*}$ with a normalization factor (call it κ). We note that it is $\chi_{l_\pi}^*$ rather than $\chi_{l_\pi}^{(\text{full})*}$ that enters into our calculation, and we choose to use the same normalization factor κ for $\chi_{l_\pi}^*$ as for $\chi_{l_\pi}^{(\text{full})*}$. Thus, in evaluating the matrix elements in Eqs. (35) and (42), we use $\kappa \chi_{l_\pi}^*$ instead of $\chi_{l_\pi}^*$. In the Δ -resonance region of our interest, it turns out that $|\kappa - 1| \lesssim 0.01$. (For neutral pion scattering, $\kappa = 1$.)

III. NUMERICAL RESULTS

A. Pion-nucleus scattering

As explained in the previous sections, our model contains four complex free parameters. Two of them are the central (V_C) and spin-orbit (V_{LS}) parts of the spreading potential [see Eq. (C5)], and the other two are the strengths, B_0 and B_1 , of the s -wave and p -wave phenomenological terms in the optical potential [see Eq. (55)]. These free parameters are optimized to fit the pion-nucleus scattering data. Because our aim here is to calculate coherent pion production off ^{12}C , we should use the $\pi^{-12}\text{C}$ scattering data to fix these parameters. Adjusting them to reproduce the total cross sections and the elastic differential

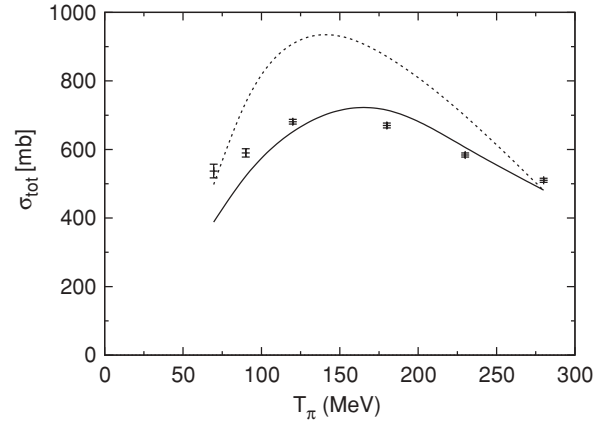


FIG. 1. Total cross sections for $\pi^{-12}\text{C}$ scattering. The solid curve was obtained with our full calculation, while the dashed curve was obtained without the spreading potential. Data are from Ref. [35].

cross sections for $\pi^{-12}\text{C}$ scattering, we obtain

$$\begin{aligned} V_C = 48.0 - 34.5i \text{ MeV}, \quad V_L = -3.0 - 2.0i \text{ MeV}, \\ B_0 = 5.1 + 5.2i \text{ MeV}, \quad B_1 = 2.8 - 5.7i \text{ MeV}. \end{aligned} \quad (60)$$

We note that our calculations include the pion-nucleus partial waves up to $l_\pi \leq 9$ [Eq. (56)] and s and p waves (and all possible spin-isospin states) for the elementary πN scattering.⁴ Figures 1 and 2 illustrate the quality of fit to the $\pi^{-12}\text{C}$ scattering data achieved in our model (with our optical potential). In Fig. 1, the total cross sections for $\pi^{-12}\text{C}$ scattering are shown as a function of the pion kinetic energy T_π in the laboratory frame. The results of our full calculation are given by the solid curve, and for comparison, the results obtained without the spreading potential are also shown by the dashed curve. We observe a large reduction in the total cross section as we go from the dashed to the solid lines, which is mainly caused by the strong pion absorption simulated by the spreading potential. In connection with fitting to the pion-nucleus scattering data, it is worthwhile to make the following comment. In the calculation of coherent pion production, the FSI is nothing but elastic scattering between the pion and the nucleus. One might therefore think that a phenomenological adjustment of the pion-nucleus optical potential to fit the elastic pion-nucleus scattering data will be good enough. However, in our consistent model building, the spreading potential enters not only into the optical potential but also into the pion production operators, and hence it is important to control its strength using the total cross-section data. The fact that the spreading potential has a very large effect on the total cross sections makes this point particularly important.

Our results for the differential cross sections are shown in Fig. 2. In addition to our full calculation, shown by the solid curve, we also show, in the dashed curve, the results obtained

⁴Hereafter, we include the same set of partial waves (l_π) in the amplitudes for both pion-nucleus scattering and pion production off a nucleus. For the nonresonant elementary pion production amplitudes, we include the partial waves up to $\ell \leq 4$ in Eq. (42).

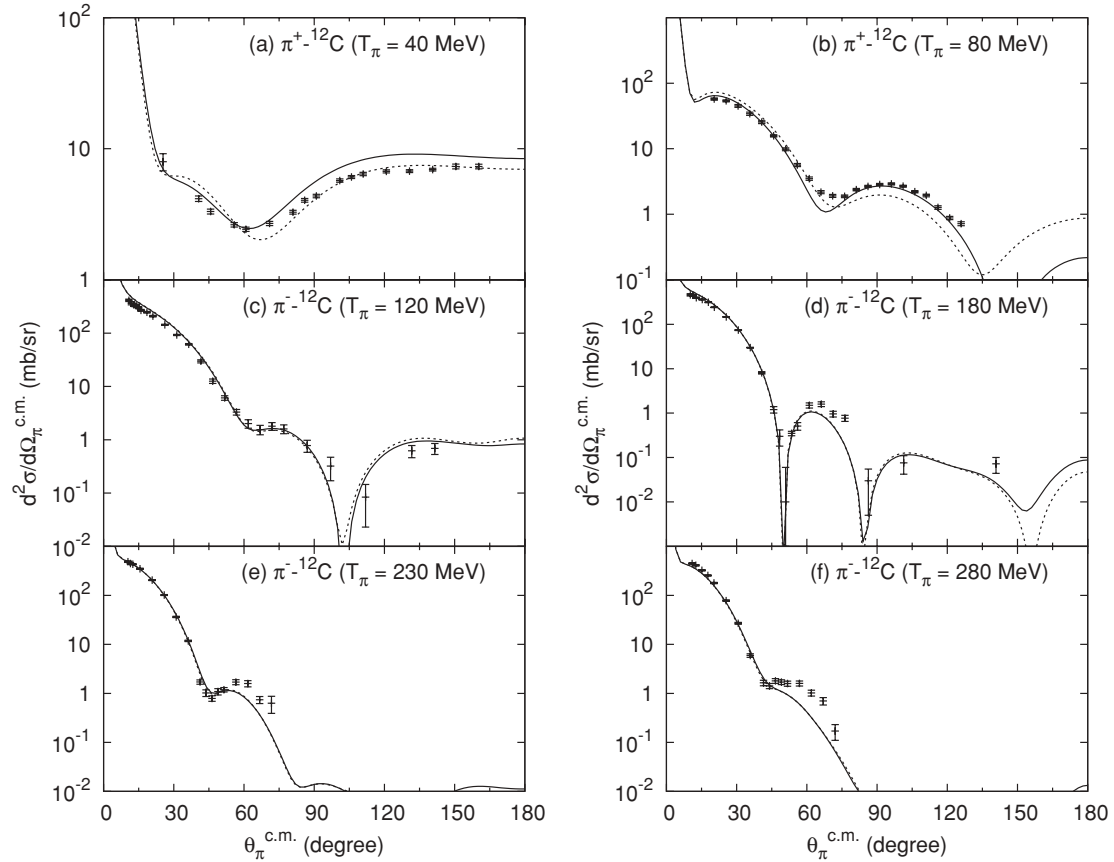


FIG. 2. π^- - ^{12}C elastic differential cross sections. The pion kinetic energy in the laboratory frame is indicated in each figure. The solid curve is obtained with our full calculation, while the dashed curve was obtained without the phenomenological terms in Eq. (54). Data are from Ref. [36] for (a), Ref. [37] for (b), and Ref. [35] for (c)–(f).

without the phenomenological term U_{ph} [see Eq. (54)]. We see that this phenomenological ρ^2 term, which simulates absorption of s -wave and p -wave pions by two-nucleons within our model, is not large in the considered $T_\pi > 40$ MeV region for π^- - ^{12}C elastic scattering. However, it is known that U_{ph} can play an important role for many observables in low-energy pion-nucleus scattering. As an example to shed light on this point, we have calculated π^- - ^{16}O elastic scattering at $T_\pi = 50$ MeV using the same model (only the nuclear density is different). We have found that, in reproducing the data satisfactorily in our approach, the ρ^2 term plays an important role, its size being almost as large as that found in Fig. 4(a) of Ref. [20]. Overall, the results of our full calculation satisfactorily reproduce the data for both the total and the elastic cross sections.

B. Coherent pion photoproduction

We are now in a position to perform a parameter-free calculation of the cross sections for coherent pion production. The photoprocess, for which extensive data are available, provides a good testing ground for checking the reliability of our approach. We compare in Fig. 3 our numerical results for the differential cross sections for $\gamma + ^{12}\text{C}_{\text{g.s.}} \rightarrow \pi^0 + ^{12}\text{C}_{\text{g.s.}}$ with the existing data [38,39]. The long-dashed lines are

obtained without FSI and without the medium effects on Δ propagation.⁵ With the medium effects on the Δ included, the short-dashed lines are obtained, and the results of our full calculation are given by the solid lines. Figure 3 indicates that the medium effects are quite sizable, and they play an important role in bringing the calculated differential cross sections in agreement with the data. Particularly noteworthy is the drastic reduction of the cross section in the Δ region [Fig. 3(c)], a feature that reflects the fact that a significant part of the medium effects simulate pion absorption. The good general agreement seen in Fig. 3 indicates the basic soundness of the method we have used in determining the spreading potential.

It is true that, for higher incident energies, in the large-angle region beyond the peak position, there are noticeable discrepancies between the results of our full calculation and the data. However, as noted in Ref. [39], the data in this region are likely to be substantially contaminated by incoherent processes in which the final nucleus is in its low-lying excited states. The effects of this type of contamination are expected to grow for higher incident photon energies and for larger momentum transfers (the large-angle region) because of

⁵The “medium effects on Δ ” here refer to the combined effects of the Pauli blocking of Δ decay (Σ_{pauli}), the spreading potential (Σ_{spr}), and the terms in square brackets in Eq. (28).

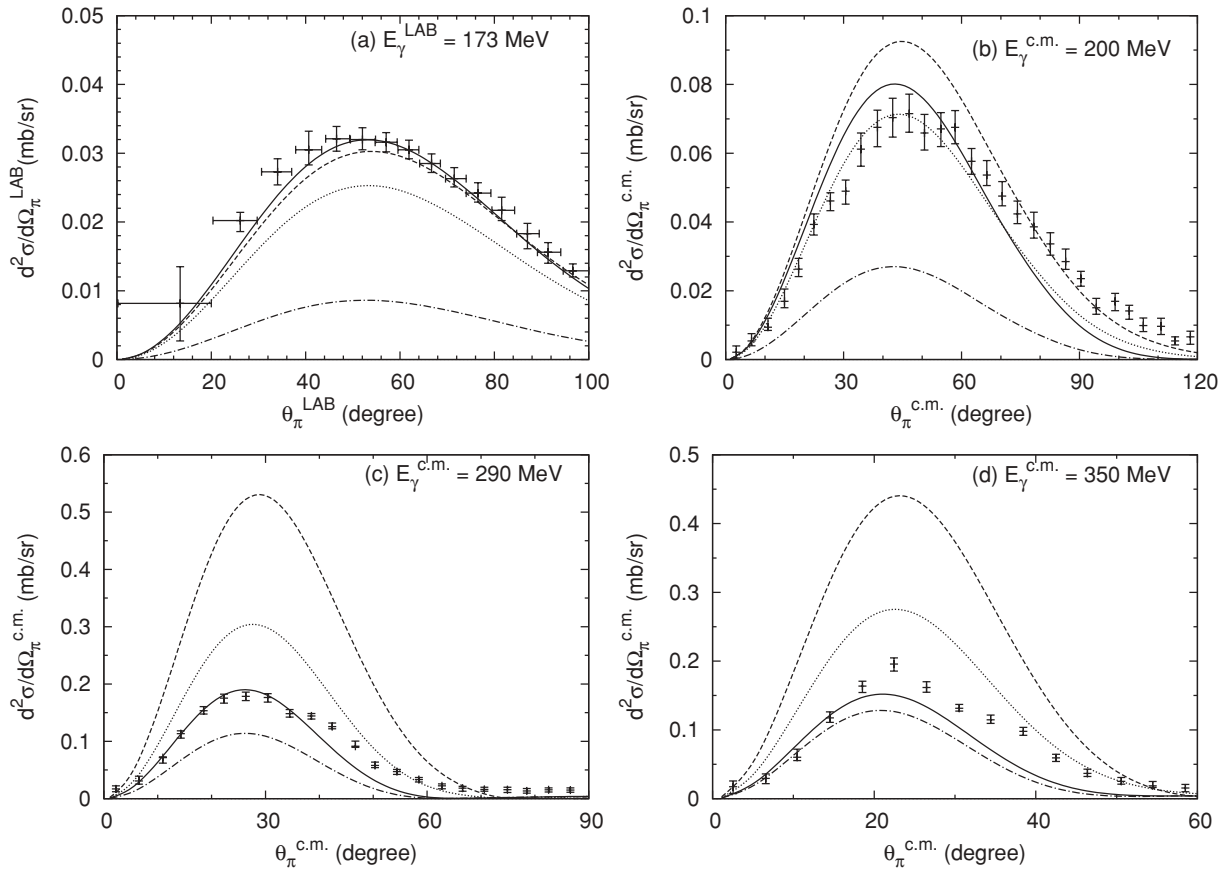


FIG. 3. Differential cross sections for $\gamma + {}^{12}\text{C}_{\text{g.s.}} \rightarrow \pi^0 + {}^{12}\text{C}_{\text{g.s.}}$ for different incident photon energies (indicated in each panel). Solid lines represent the results of the full calculation. Dashed lines were obtained without the FSI and without the medium effects on the Δ -propagation, while dotted lines were obtained with the medium effects on the Δ included. Dash-dotted curves correspond to a case in which the pion production operator includes only the Δ mechanism. For more detailed explanations for the different cases, see the text. Data are from Ref. [38] for (a) and from Ref. [39] for (b)–(d).

increased nuclear excitations. We therefore take the viewpoint that the discrepancy found in Fig. 3(b) to Fig. 3(d) does not necessarily signal a failure of our model and that our model describes coherent pion photoproduction reasonably well.

Figure 3 also shows (in the dash-dotted lines) the results corresponding to a case in which the pion production operator includes only the Δ mechanism (the nonresonant mechanism turned off);⁶ the distorted pion wave function incorporating FSI is the same as that used for the full calculation. These results serve to demonstrate the importance of the nonresonant mechanism. Figure 3(a) indicates that, near threshold, the contributions from the resonant and nonresonant mechanisms are comparable, a feature that is not surprising away from the resonance peak. A remarkable feature is that, even near the resonance energy [see Fig. 3(c)], the contribution from the nonresonant mechanism is quite significant. This is partly because the resonant contribution is considerably suppressed

by pion absorption (the spreading potential) and the nonlocal effect of Δ propagation (the Δ kinetic term).⁷

To summarize this section, the results for the coherent photo-pion production process establish, to a satisfactory degree, the reliability of our present approach (i.e., combined use of the SL model and the Δ -hole model) and motivate us to apply the same approach to neutrino-induced coherent pion production.

C. Neutrino-induced coherent pion production

We now present the numerical results of our calculations for neutrino-induced coherent pion production on the ${}^{12}\text{C}$ target. We consider the CC and NC processes induced by a neutrino or an antineutrino:

$$\begin{aligned} \nu_\mu + {}^{12}\text{C}_{\text{g.s.}} &\rightarrow \mu^- + \pi^+ + {}^{12}\text{C}_{\text{g.s.}}, \\ \nu + {}^{12}\text{C}_{\text{g.s.}} &\rightarrow \nu + \pi^0 + {}^{12}\text{C}_{\text{g.s.}}, \end{aligned}$$

⁶In the SL model, the resonant amplitude itself contains the nonresonant mechanism. We refer to the purely nonresonant amplitudes as “nonresonant amplitudes,” and it is only these nonresonant amplitudes that we turn off here and, later, in Figs. 5–8 and 10.

⁷We come back to the nonlocal effect owing to the Δ kinetic term later when we discuss neutrino-induced processes.

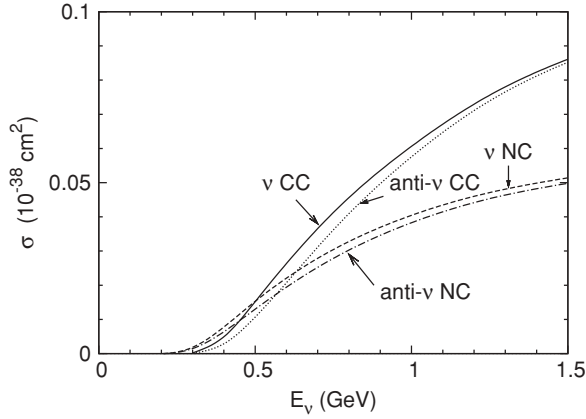


FIG. 4. E_ν dependence of the total cross section for $\nu_\mu + {}^{12}\text{C}_{\text{g.s.}} \rightarrow \mu^- + \pi^+ + {}^{12}\text{C}_{\text{g.s.}}$ (solid line), $\nu + {}^{12}\text{C}_{\text{g.s.}} \rightarrow \nu + \pi^0 + {}^{12}\text{C}_{\text{g.s.}}$ (dashed line), $\bar{\nu}_\mu + {}^{12}\text{C}_{\text{g.s.}} \rightarrow \mu^+ + \pi^- + {}^{12}\text{C}_{\text{g.s.}}$ (dotted line), and $\bar{\nu} + {}^{12}\text{C}_{\text{g.s.}} \rightarrow \bar{\nu} + \pi^0 + {}^{12}\text{C}_{\text{g.s.}}$ (dash-dotted line).

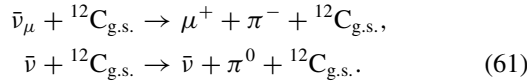


Figure 4 gives the total cross sections for these processes as functions of the incident neutrino (antineutrino) energy in the laboratory system E_ν . It is shown that, for higher incident energies, the ratio σ_{CC}/σ_{NC} approaches 2, a value expected from the isospin factor. For lower incident energies ($E_\nu \lesssim 500$ MeV), however, σ_{NC} is larger than σ_{CC} , reflecting the fact that the phase space for the CC process is reduced significantly by the muon mass. It is well known that interference between the vector and the axial-vector currents can lead to different cross sections for the neutrino and antineutrino processes. However, because the coherent process is dominated by the contribution of the axial current (see Fig. 9), the role of the interference term is diminished drastically. This explains why in Fig. 4 the cross sections for the neutrino and antineutrino processes are almost the same.

To compare our results with data, we need to evaluate the total cross sections averaged over the neutrino fluxes that pertain to the relevant experiments. We choose to use the fluxes up to $E_\nu \leq 2$ GeV and neglect the fluxes beyond that limit based on the following consideration. Because our model includes no resonances other than the Δ , it is expected to be reliable only for $W \lesssim 1.4$ GeV. The fact that even at $E_\nu = 1$ GeV coherent pion production can involve contributions coming from the $W > 1.4$ GeV region is disquieting, but we can still expect that the Δ -excitation contribution is predominant for the total cross section for the coherent process. (This feature can be seen in, for example, Fig. 5, discussed later.) For $E_\nu \sim 2$ GeV, we do expect that Δ dominance gets significantly less pronounced but that Δ still gives the most important contribution. Meanwhile, the region $E_\nu \gtrsim 1.5$ GeV belongs to the tail of the neutrino flux used in MiniBooNE. We therefore consider it reasonable to compare with data our theoretical cross section averaged over the neutrino flux up to $E_\nu = 2$ GeV. For the CC process, we use the flux reported in Ref. [40]

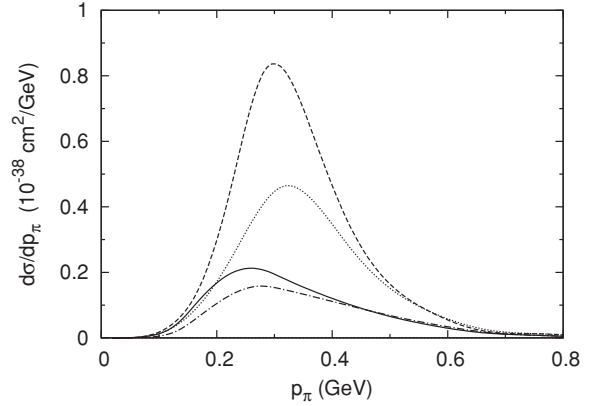


FIG. 5. Pion momentum distribution for $\nu_\mu + {}^{12}\text{C}_{\text{g.s.}} \rightarrow \mu^- + \pi^+ + {}^{12}\text{C}_{\text{g.s.}}$ at $E_\nu = 1$ GeV; p_π is the pion momentum in the laboratory frame. Solid, dashed, dotted, and dash-dotted lines follow the same convention as in Fig. 3.

and deduce

$$\sigma_{\text{ave}}^{\text{CC}} = 6.3 \times 10^{-40} \text{ cm}^2. \quad (62)$$

A K2K experiment [1] reports the upper limit

$$\sigma_{\text{K2K}} < 7.7 \times 10^{-40} \text{ cm}^2. \quad (63)$$

In fact, this upper limit corresponds to events satisfying the muon momentum cut, $p_\mu > 450$ MeV, and the cut on the momentum transfer squared, $Q_{\text{rec}}^2 < 0.1$ GeV²; Q_{rec}^2 is calculated as

$$Q_{\text{rec}}^2 = 2E_\nu^{\text{rec}}(E_\mu - p_\mu \cos \theta_\mu) - m_\mu^2, \quad (64)$$

where the reconstructed neutrino energy (E_ν^{rec}) is calculated from the muon kinematics [the energy (E_μ) and the scattering angle (θ_μ)] assuming the quasielastic kinematics:

$$E_\nu^{\text{rec}} = \frac{1}{2} \frac{(m_p^2 - m_\mu^2) - (m_n - V)^2 + 2E_\mu(m_n - V)}{(m_n - V) - E_\mu + p_\mu \cos \theta_\mu}, \quad (65)$$

where m_p , m_n , and m_μ are the masses of the proton, neutron, and muon, respectively, and the nuclear potential (V) is set to 27 MeV. Our result in Eq. (62) is also obtained with these cuts and is consistent with the K2K data. We note that a recent report from SciBooNE [2] gives a similar empirical upper limit.

For the NC process, we use the flux reported by MiniBooNE in Ref. [41] and arrive at

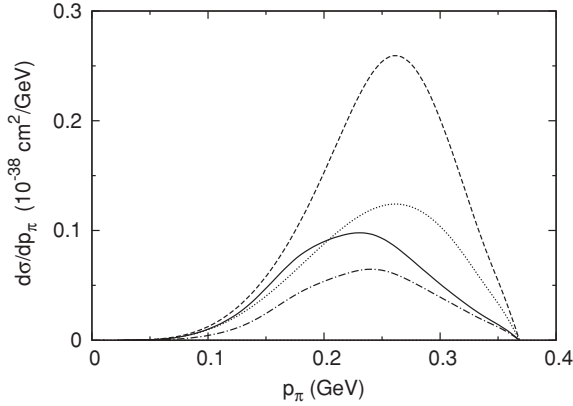
$$\sigma_{\text{ave}}^{\text{NC}} = 2.8 \times 10^{-40} \text{ cm}^2. \quad (66)$$

This is to be compared with

$$\sigma_{\text{MiniBooNE}} = 7.7 \pm 1.6 \pm 3.6 \times 10^{-40} \text{ cm}^2, \quad (67)$$

given in Ref. [42]. Our result is consistent with the empirical value within the large experimental errors, even though the theoretical value is rather visibly smaller than the empirical central value. It must be noted, however, that Ref. [42] is a preliminary report and that, as discussed in great detail in Ref. [7], $\sigma_{\text{MiniBooNE}}$ may be overestimated owing to the use of the RS model [6] in the analysis.

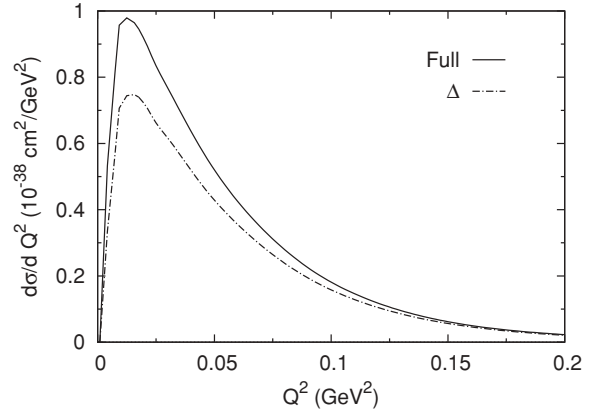
We now proceed to present our results for differential observables. In view of the fact that the event rates

FIG. 6. Same as Fig. 5 but for $E_\nu = 0.5$ GeV.

(cross section \times flux) in the K2K, MiniBooNE, and SciBooNE experiments [3,40] have been reported to have a peak around $E_\nu \sim 1$ GeV, we often use this energy as a representative in the following presentation. Meanwhile, because the neutrino flux in the planned T2K experiment is expected to have a peak around $E_\nu = 0.6\text{--}0.7$ GeV [43], we also present results for lower neutrino energies when that seems useful.

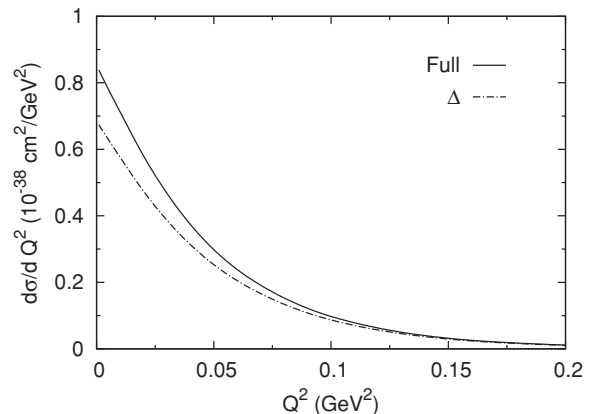
The pion momentum spectrum for CC neutrino-induced coherent pion production is shown in Fig. 5 (Fig. 6) for $E_\nu = 1$ GeV (0.5 GeV). The importance of the medium effects manifests itself here in the same manner as in the photoprocess (Fig. 3). In the Δ region, strong pion absorption is seen to reduce the cross sections significantly, and FSI shifts the peak position. The dash-dotted line corresponds to a case in which the pion production operator contains only the Δ mechanism (without nonresonant contributions), while the pion optical potential is kept unchanged. We note that, at $E_\nu = 1$ GeV (0.5 GeV), the dash-dotted line corresponds to 82% (64%) of the solid line (the results of the full calculation). We have seen in the photoprocess that the nonresonant mechanism is more important for a smaller energy transfer. To what extent the neutrino case should share this feature is not obvious because the axial-vector current contributions dominate here (see Fig. 9). However, Figs. 5 and 6 show that, in the neutrino case as well, the differential cross sections with smaller pion momenta are more enhanced by the nonresonant mechanism and that this feature is more prominent for a smaller value of E_ν . A similar tendency is seen for the NC process also. These results indicate that the nonresonant amplitudes in our model, which are dressed by the rescattering, play a significant role in coherent pion production; their role is particularly important for $E_\nu \lesssim 0.5$ GeV. This characteristic feature of our model should be contrasted with the fact that (tree-level) nonresonant mechanisms play essentially no role in any of the previous microscopic calculations for neutrino-induced coherent pion production. A more detailed comparison of the elementary amplitudes used in our present calculation and the previous microscopic-model calculations is given in Sec. III E.

We show in Fig. 7 (Fig. 8) the Q^2 distribution for the CC (NC) process. Note that Q^2 defined by $Q^2 \equiv -q^2 \equiv -(p_\nu - p'_\ell)^2$ is different from Q_{rec}^2 defined in Eq. (64). Because

FIG. 7. Q^2 spectrum for $\nu_\mu + {}^{12}\text{C}_{\text{g.s.}} \rightarrow \mu^- + \pi^+ + {}^{12}\text{C}_{\text{g.s.}}$ at $E_\nu = 1$ GeV.

of the nuclear form factor effect, the distribution rises sharply as Q^2 approaches 0; for the CC process, however, the Q^2 distribution becomes 0 at $Q^2 = 0$ owing to the finite muon mass. Here, again, we show the results corresponding to a case in which the pion production operator contains only the Δ effect (with nonresonant contributions turned off). The nonresonant mechanism is seen to change the spectrum shape significantly and lead to a sharper peak.

It is informative to examine the individual contributions of the vector and axial-vector currents. We show in Fig. 9 these individual contributions to the neutrino CC process. We find strong dominance of the axial-vector current. The nuclear form factor causes drastic suppression of nonforward pion production. This aspect, combined with the fact that the transverse photon coupling of the vector current [Eq. (7)] forbids forward pion production, leads to strong suppression of the vector current contribution. By contrast, because the vertex structure of the axial-vector current favors forward pion production, the strong suppression mechanism at work for the vector current does not apply here. This is the reason why the axial-vector current dominates. This result may be used to argue that incoherent pion production processes in which a nucleus does not break up, but transits to excited states, are much less important than coherent pion production in neutrino-nucleus scattering. As shown in Fig. 3, incoherent

FIG. 8. Same as Fig. 7 but for the NC process at $E_\nu = 1$ GeV.

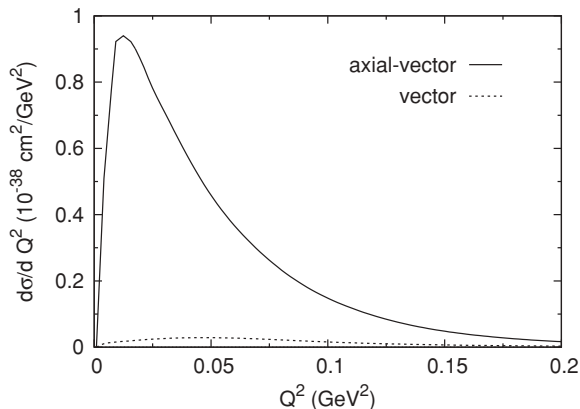


FIG. 9. Contributions from the axial-vector (solid) and vector (dashed) currents for $\nu_\mu + {}^{12}\text{C}_{\text{g.s.}} \rightarrow \mu^- + \pi^+ + {}^{12}\text{C}_{\text{g.s.}}$ at $E_\nu = 1$ GeV.

processes make considerable contributions to the total pion production in the photoprocess,⁸ a feature that may lead to the expectation that incoherent processes are considerable in the neutrino process as well. However, the mechanism responsible for the axial-vector dominance in the neutrino process works for the photoprocess in such a manner that coherent photo-pion production is strongly suppressed. Also, the inelastic transition form factor has a peak at a nonzero momentum transfer. As a result, for the photoreaction, the contributions from the incoherent processes become comparable to those from the coherent process. Thus the importance of incoherent processes relative to the coherent process can be very different between the photo- and the neutrino processes. Takaki *et al.* [44] used a similar argument to explain a significant (very small) contribution from incoherent processes in photopion production (pion-nucleus scattering), compared to the coherent process. This argument may serve as a justification for the assumption currently used in data analyses that incoherent processes need not be taken into account explicitly.

Finally, we examine the effect of the nonlocality of Δ propagation in nuclei; because we employed the local density approximation to evaluate the Δ Green function [Eq. (17)], this effect arises only from the Δ kinetic term in the Δ Hamiltonian [Eq. (25)]. Although, as mentioned in the Introduction, this subject has been studied in Ref. [21], that study only included the Δ mechanism, without considering FSI or medium effects on the Δ . It is thus interesting to revisit this problem in the framework of our significantly extended treatment. In the local approximation, we neglect the kinetic term in the Δ Hamiltonian [Eq. (25)], which means that the Δ is considered to be so heavy that it does not propagate in nuclear medium. To facilitate our discussion, we introduce the ratio $\mathcal{R}(E_\nu)$, defined by

$$\mathcal{R}(E_\nu) \equiv \sigma(E_\nu)/\sigma_{\text{local}}(E_\nu), \quad (68)$$

⁸The contributions from incoherent processes are larger than they appear in Fig. 3 because $\sin\theta_\pi$ needs to be multiplied in integrating over θ_π .

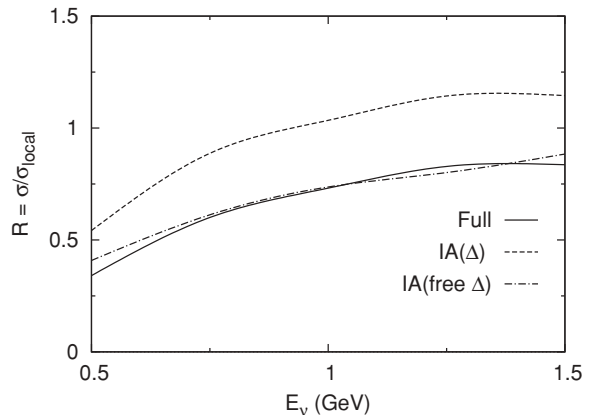


FIG. 10. Effect of the nonlocality of Δ propagation for $\nu_\mu + {}^{12}\text{C}_{\text{g.s.}} \rightarrow \mu^- + \pi^+ + {}^{12}\text{C}_{\text{g.s.}}$. The ratio \mathcal{R} of the total cross sections was obtained with and without taking account of the nonlocal effect.

where $\sigma(E_\nu)$ represents the total cross section for $\nu_\mu + {}^{12}\text{C}_{\text{g.s.}} \rightarrow \mu^- + \pi^+ + {}^{12}\text{C}_{\text{g.s.}}$ calculated with the Δ propagator including the Δ kinetic term, whereas $\sigma_{\text{local}}(E_\nu)$ is that obtained in the local approximation. Figure 10 shows $\mathcal{R}(E_\nu)$ values calculated for the various cases. The long-dashed curve corresponds to the Δ -only case (without FSI or medium effects on the Δ ; see footnote 5), and the solid line to the case that includes the nonresonant components, medium effects on the Δ , and FSI. To make a comparison with Ref. [21], we first consider the long-dashed line; $\mathcal{R}(E_\nu)$ in this case is found to be 0.55, 1.03, and 1.14 at $E_\nu = 0.5, 1.0,$ and 1.5 GeV. Meanwhile, Ref. [21] reports $\mathcal{R}(E_\nu) \lesssim 0.5, 0.6,$ and $\lesssim 1$ at $E_\nu = 0.5, 1.0,$ and 1.5 GeV. Although both calculations indicate that the nonlocal effects are important, our results are qualitatively different from those of Ref. [21]. This difference originates from different ways of treating the energy in the Δ propagator. In Ref. [21], the in-medium Δ propagator is assumed to be the same as the free Δ propagator, whereas our Δ propagator [$G_{\Delta h}$; Eq. (17)] is a nuclear many-body operator [25] (with some of the medium effects switched off). To illustrate this point, we include in Fig. 10 (dash-dotted line) the results obtained with the use of the free Δ propagator. In this case, we find $\mathcal{R}(E_\nu) = 0.4, 0.76,$ and 0.88 at $E_\nu = 0.5, 1.0,$ and 1.5 GeV, which is fairly close to the results in Ref. [21]. The result shown by the solid line indicates that, after the sophistication of the calculation, the nonlocality owing to the kinetic term is still important over the entire range of E_ν under consideration. In the previous microscopic calculations for neutrino-induced coherent pion production, the nonlocality has not been explicitly taken into account. However, this does not necessarily mean that the earlier results are off by an amount suggested by comparison of the curves in Fig. 10, for it is possible that the nonlocality effects are partly included with the use of the spreading potential fitted to observables. In view of the importance of the nonlocal effect, however, we consider it preferable to take it into account explicitly, rather than include it operationally in the Δ mass shift.

An additional point of interest is that it was reported in Ref. [21] that the nonlocality changes the shapes of the

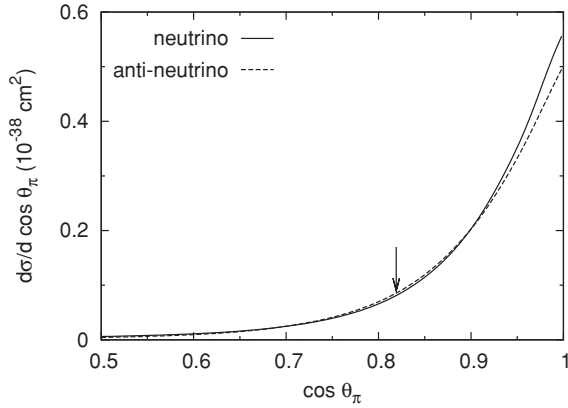


FIG. 11. The $\cos \theta_\pi$ distribution for $\nu_\mu + {}^{12}\text{C}_{\text{g.s.}} \rightarrow \mu^- + \pi^+ + {}^{12}\text{C}_{\text{g.s.}}$ and $\bar{\nu}_\mu + {}^{12}\text{C}_{\text{g.s.}} \rightarrow \mu^+ + \pi^- + {}^{12}\text{C}_{\text{g.s.}}$ at $E_\nu = 1$ GeV. The position of $\theta_\pi = 35^\circ$ is indicated by the arrow.

differential cross sections. We remark that our results (not shown here) agree with that finding.

D. Comparison with SciBooNE and MiniBooNE data

The SciBooNE collaboration has been pursuing a further analysis of the data on neutrino and antineutrino CC coherent pion production, and some preliminary results have appeared in Refs. [5] and [45]. These results contain detailed information on the differential observables for the pion and muon, and it seems informative to present our theoretical results in a manner that allows ready comparison with these data. To this end, we need to take into account the muon momentum cut ($p_\mu > 350$ MeV) and the momentum transfer cut ($Q_{\text{rec}}^2 < 0.1$ GeV²) adopted in the SciBooNE experiment; Q_{rec}^2 has been defined in Eq. (64). The theoretical results we present in the following take account of these cuts unless otherwise stated. We present the results at $E_\nu = 1$ GeV, around which the event rate has a peak. Although for direct comparison, we need to convolute the observables with the (anti-) neutrino flux used in the SciBooNE experiment, the flux has not been released yet. We therefore present our results at a representative value of $E_\nu = 1$ GeV. In Fig. 11, we show the $\cos \theta_\pi$ distribution for the neutrino and antineutrino CC processes. In the recent data analysis by the SciBooNE collaboration, events are classified according to the pion emission angle (θ_π). Their preliminary results exhibit a rather clear excess yield for $\theta_\pi < 35^\circ$, which is thought to be ascribable to coherent pion production. In our model, 85% of the pions are emitted in $\theta_\pi < 35^\circ$ for the neutrino CC process at $E_\nu = 1$ GeV, a feature that is in fair agreement with the preliminary SciBooNE result.

Next we show, in Fig. 12 (solid line), the Q_{rec}^2 distribution for the neutrino reaction.⁹ Only the p_μ cut is applied here for an obvious reason. We can see that the contribution from above $Q_{\text{rec}}^2 = 0.1$ GeV² (the value adopted for the Q_{rec}^2 cut) constitutes only a small fraction of the entire contribution (3% for the solid curve). The decomposition of the total contribution (solid

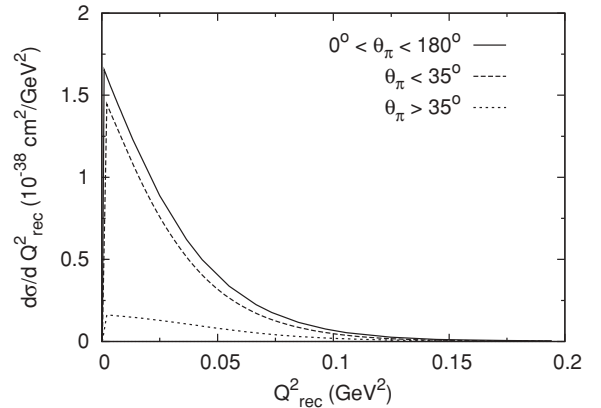


FIG. 12. Q_{rec}^2 distribution for $\nu_\mu + {}^{12}\text{C}_{\text{g.s.}} \rightarrow \mu^- + \pi^+ + {}^{12}\text{C}_{\text{g.s.}}$ at $E_\nu = 1$ GeV.

curve) into two parts according to whether θ_π is smaller or larger than 35° is shown by the dashed curve ($\theta_\pi < 35^\circ$) or the dotted curve ($\theta_\pi > 35^\circ$), respectively. The pion and muon momentum distributions are shown in Figs. 13 and 14. The upper (lower) end of the pion (muon) momentum distribution is sharply cut off because of the muon momentum cut ($p_\mu > 350$ MeV). The muon scattering angle distribution is shown in Fig. 15. Figures 11–15 clearly show the characteristics of coherent pion production, that is, sharply forward scattering (emission) of the muon (pion) with small momentum transfers. Finally, in Fig. 16 we show the spectrum with respect to the coplanar angle difference $\Delta\phi$, which is defined by $\Delta\phi = \phi_\pi - \pi$, where ϕ_π is the pion azimuthal angle in the LAB frame. (See Fig. 17 for a graphical representation of $\Delta\phi$.)

Figure 16 shows slight asymmetry in the $\Delta\phi$ distribution around $\Delta\phi = 0$. It is interesting to note that this asymmetry is generated mostly by the contribution from the nonresonant amplitudes. To demonstrate this point, we present in the same figure the results obtained with the nonresonant amplitudes turned off (dash-dotted curve). We also remark that the asymmetry arises mostly from the kinematical region satisfying $\theta_\pi > 35^\circ$ (see dotted curve). A similar asymmetry also arises for the antineutrino process.

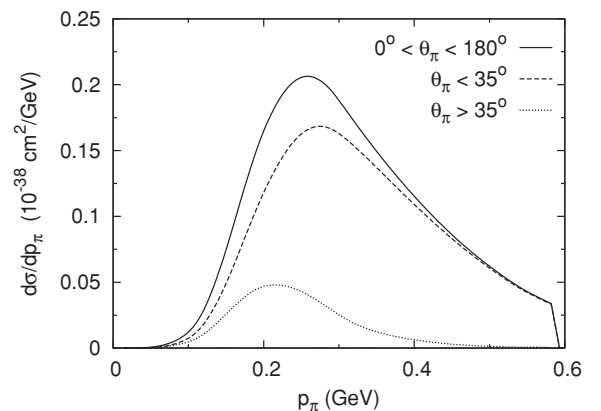


FIG. 13. Pion momentum distribution for $\nu_\mu + {}^{12}\text{C}_{\text{g.s.}} \rightarrow \mu^- + \pi^+ + {}^{12}\text{C}_{\text{g.s.}}$ at $E_\nu = 1$ GeV.

⁹As discussed earlier, the neutrino and antineutrino cross sections differ only slightly.

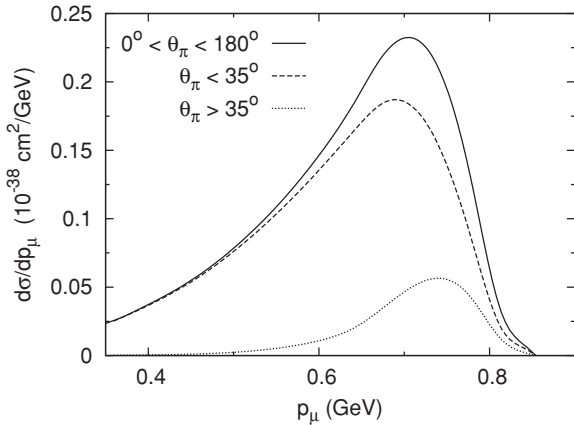


FIG. 14. Muon momentum distribution for $\nu_\mu + {}^{12}\text{C}_{\text{g.s.}} \rightarrow \mu^- + \pi^+ + {}^{12}\text{C}_{\text{g.s.}}$ at $E_\nu = 1$ GeV.

The SciBooNE collaboration has recently presented its preliminary results corresponding to Figs. 11–16 for both the neutrino and the antineutrino CC coherent pion production reactions [5,45]. When the flux prediction for the SciBooNE experiment becomes available, we will be able to convolute the results of our calculation with the flux and make direct comparison with the data.

Meanwhile, the MiniBooNE collaboration has been investigating the NC process in (anti-) neutrino-nucleus scattering; some results for the neutrino process have been published [3], and more results are expected to be released. Because the neutrino flux information for the MiniBooNE experiment is available [41], we can give the theoretical values of relevant observables convoluted with the flux. At present, data are publicly available only for the η distribution [$\eta \equiv E_\pi(1 - \cos\theta_\pi)$], and we compare our calculation for this quantity with the data. In the analysis of the MiniBooNE NC data, the η distribution was used to distinguish coherent pion production from other processes contributing to the π^0 -production events. To be more specific, MiniBooNE used the “shape” of the η distribution obtained from the RS model [6] with the momentum reweighting function applied. It has been found, however, that a microscopic calculation in Ref. [7] gives an

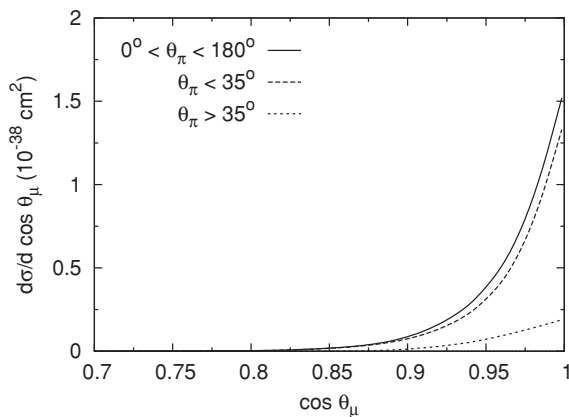


FIG. 15. Muon scattering angle distribution for $\nu_\mu + {}^{12}\text{C}_{\text{g.s.}} \rightarrow \mu^- + \pi^+ + {}^{12}\text{C}_{\text{g.s.}}$ at $E_\nu = 1$ GeV.

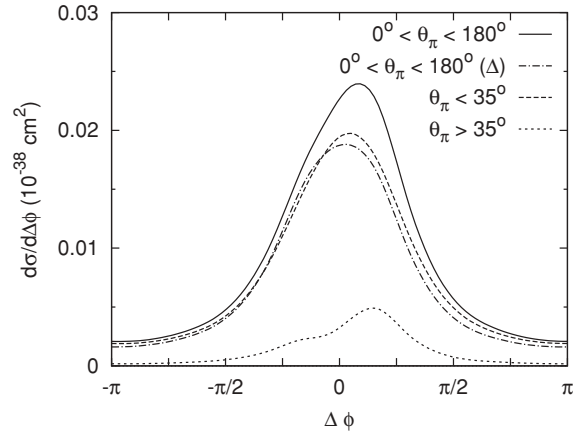


FIG. 16. Coplanar angle difference ($\Delta\phi$) distribution for $\nu_\mu + {}^{12}\text{C}_{\text{g.s.}} \rightarrow \mu^- + \pi^+ + {}^{12}\text{C}_{\text{g.s.}}$ at $E_\nu = 1$ GeV. The definition of $\Delta\phi$ is given in Fig. 17.

η distribution appreciably different from that obtained in the RS model, and the authors of Ref. [7] have pointed out that the MiniBooNE might have substantially overestimated the NC events. Figure 18 shows the “average” η distribution obtained by convoluting the η distribution given by our present calculation with the MiniBooNE neutrino flux [41]. For comparison, the figure also shows the MiniBooNE Monte Carlo results (cf. Fig. 3(b) of Ref. [3]), arbitrarily rescaled to match the theoretical curve at $\eta = 0.005$ GeV. We remark that the η distribution we have obtained is fairly close to that given in Ref. [7], because the nonresonant amplitudes do not change the shape of the η distribution significantly. Therefore, we arrive at the same conclusion as in Ref. [7], that it is possible that MiniBooNE substantially overestimated the NC events.

To facilitate a comparison of our calculation with data that are expected to become available soon from MiniBooNE, we present theoretical predictions for some more quantities that are likely to be relevant. Figure 19 shows the flux-convoluted π^0 -momentum distribution predicted by our calculation. As far as observables for the antineutrino process are concerned, the flux-convoluted η distribution resulting from our calculation is given in Fig. 20, and the flux-convoluted π^0 -momentum distribution obtained in our model is shown in Fig. 21.

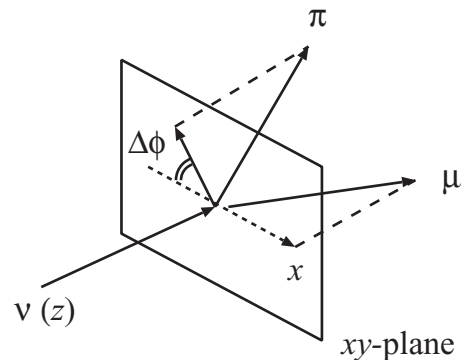


FIG. 17. Graphical definition for the coplanar angle difference ($\Delta\phi$).

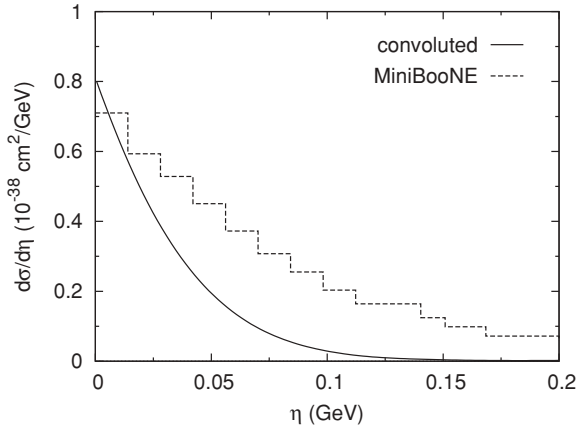


FIG. 18. Flux-convoluted η distribution for $\nu + {}^{12}\text{C}_{\text{g.s.}} \rightarrow \nu + \pi^0 + {}^{12}\text{C}_{\text{g.s.}}$ obtained in our full calculation. The neutrino flux is taken from MiniBooNE [41]. Also shown is the Monte Carlo result from MiniBooNE [3] rescaled to match our result at $\eta = 0.005$ GeV.

E. Comparison of microscopic models

As mentioned, there are mainly two theoretical approaches to coherent pion production in neutrino-nucleus scattering: a PCAC-based model and a microscopic model. The relation between the RS model (a PCAC-based model) and a microscopic model has been discussed in great detail in Ref. [7], and comparison of those two models, including some improvement of the RS model, has been made in Refs. [7] and [8]. The authors of Refs. [7] and [8] have emphasized that it can be problematic to use the RS model for $E_\nu \lesssim 2$ GeV. To shed some more light on this issue, we consider it useful to compare different microscopic models. In particular, we focus here on comparison between our model and the model of Amaro *et al.* [7], which is the most sophisticated among the existing microscopic models for neutrino-induced coherent pion production.¹⁰ The other microscopic calculations in the literature lack one or more aspects that are obviously important, such as the distortion of the final pion and the nonresonant mechanism for the weak currents.

Here, we focus particularly on the elementary amplitudes for pion production off the nucleon. Our approach employs the SL model, while Amaro *et al.* [7] used a model developed in Ref. [47] (referred to as HNV). Both SL and HNV include the resonant and nonresonant amplitudes. A point to be noted, however, is that, although both models reproduce reasonably well the data for the $\nu_\mu + N \rightarrow \mu^- + \pi^+ + N$ reactions after an appropriate adjustment of the axial- $N\Delta$ coupling, the two models involve rather different reaction mechanisms. In the SL model, we derive a set of tree diagrams from a given Lagrangian with the use of a unitary transformation, and then we embed these tree diagrams in the LS equation, which is solved exactly to yield a nonperturbative pion production amplitude that satisfies π - N two-body unitarity. In HNV, on

¹⁰A rather extensive comparison of numerical results from various calculations of neutrino-induced coherent pion production, including those of Amaro *et al.* [7], recent PCAC-based models [12,13], and ours, was presented at NuInt09 by Boyd *et al.* [46].

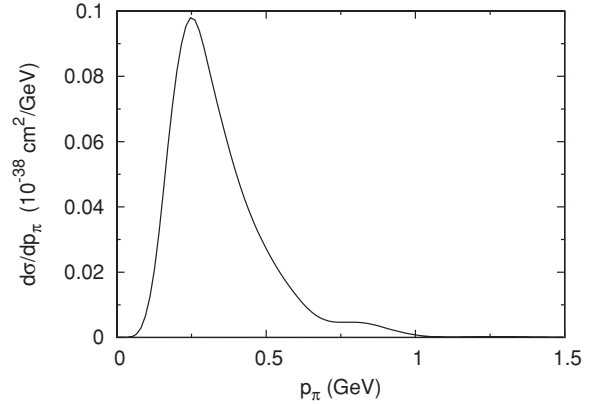


FIG. 19. Flux-convoluted π^0 -momentum distribution for $\nu + {}^{12}\text{C}_{\text{g.s.}} \rightarrow \nu + \pi^0 + {}^{12}\text{C}_{\text{g.s.}}$. The neutrino flux is taken from MiniBooNE [41].

the other hand, a set of tree diagrams is calculated from a chiral Lagrangian. Then the sum of the contributions of these tree diagrams is identified with the pion production amplitude. At the tree level, the SL and the HNV models have essentially the same nonresonant mechanisms; a contact vertex in HNV may be interpreted as the vector-meson exchange mechanism in SL. However, the role of the nonresonant amplitude appears differently in the two models. In the SL model, the nonresonant amplitude contributes constructively (destructively) to resonant amplitudes below (above) the resonance energy. For $\nu_\mu + p \rightarrow \mu^- + \pi^+ + p$, the interference of the nonresonant amplitude with the resonant amplitude changes the total cross sections in the SL model by a factor of 1.5, 1.02, and 0.96 at $E_\nu = 0.5, 1, \text{ and } 1.5$ GeV,¹¹ while the interference in the HNV always enhances the total cross sections, for example, enhancement by a factor of 1.1 at $E_\nu = 1.5$ GeV. The difference in the nonresonant mechanism appears also in the coherent pion production on ${}^{12}\text{C}$, where only the spin and isospin nonflip amplitude contributes. Whereas the nonresonant amplitude plays an important role in our model

¹¹See footnote 6.

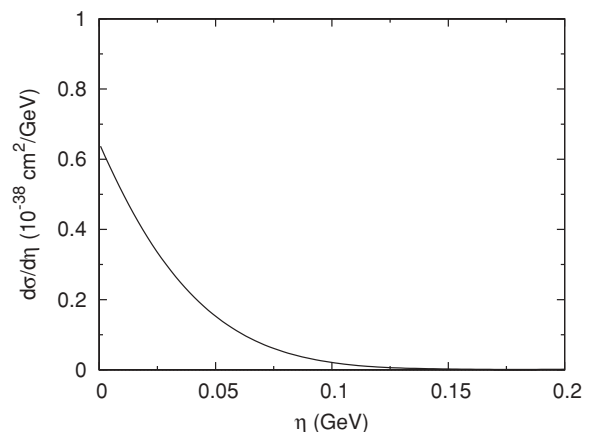


FIG. 20. Flux-convoluted η distribution for $\bar{\nu} + {}^{12}\text{C}_{\text{g.s.}} \rightarrow \bar{\nu} + \pi^0 + {}^{12}\text{C}_{\text{g.s.}}$. The antineutrino flux is taken from MiniBooNE [41].

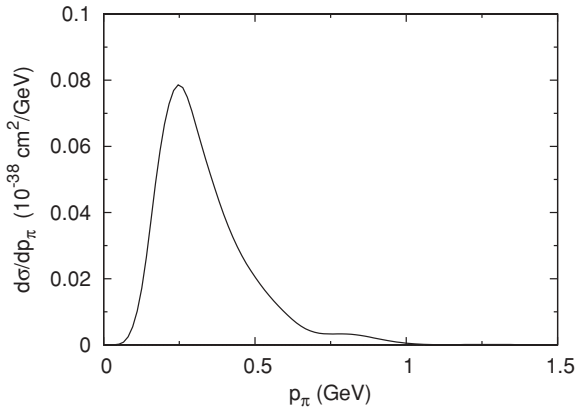


FIG. 21. Flux-convoluted π^0 -momentum distribution for $\bar{\nu} + {}^{12}\text{C}_{\text{g.s.}} \rightarrow \bar{\nu} + \pi^0 + {}^{12}\text{C}_{\text{g.s.}}$. The antineutrino flux is taken from MiniBooNE [41].

(as shown in Figs. 5 and 6), it plays essentially no role in the HNV model. In neutrino CC coherent pion production, the full (tree) nonresonant amplitude increases the total cross section by 36% (19%) at $E_\nu = 0.5$ GeV and 18% (0.4%) at $E_\nu = 1$ GeV in our model. Thus the nonresonant mechanism in the spin-isospin nonflip amplitude is enhanced by the rescattering process. In the SL model, the nonresonant and resonant πN dynamics in the Δ -resonance region has been tested using the extensive data on (γ, π) and $(e, e'\pi)$ reactions. Although the SL model, which provides a unified description of the electroweak pion production reactions, describes very well the available data on the $(\nu, \ell\pi)$ processes, the current data do not yet allow testing of the details of the reaction mechanism.

Furthermore, utilizing the consistency of $(\nu, \ell\pi)$, $(e, e'\pi)$, and (π, π) reactions in the SL model, we have developed a model that treats photo- and neutrino-induced coherent pion production processes in a unified manner. Thus we were able to calibrate the reliability of our approach with data for the photoprocesses, which is an aspect specific to our approach.

IV. CONCLUSIONS

We have developed a microscopic dynamical model for describing neutrino-induced coherent pion production on nuclei. Because experimental data for neutrino (both elementary and nuclear) processes are rather limited, it is not straightforward to assess the reliability of theoretical calculations. A reasonable strategy seems to develop a model that describes strong and electroweak processes in a unified way and then to test the model extensively by comparison with a large collection of data for the strong-interaction and photo-induced processes and with limited available data for weak processes. We have carried out this program here for the case of the neutrino-induced coherent pion production process. By virtue of the mentioned strategy, our model is probably the most extensively tested among the existing models for this process. To achieve the stated goal, we need a theoretical framework that provides a unified description for the elementary (π, π') , (γ, π) , and $(\nu, \ell\pi)$ processes on a single nucleon. We have adopted the SL model, which is known to give satisfactory descriptions

of these elementary amplitudes. We then have combined the SL model with the Δ -hole model to construct a theoretical framework that can describe pion-nucleus scattering and electroweak coherent pion production in a unified way. The unified nature of this approach allows us to fix free parameters in the model using the data for pion-nucleus scattering, which in turn enables us to make parameter-free predictions of electroweak coherent pion production off a nucleus. Another benefit of the present unified approach is that we can assess the reliability of our model by comparing the results for coherent pion photo-production with the data. Our model is found to describe reasonably well both pion-nucleus scattering and coherent photoprocesses, which establishes a basis for applying the same model to neutrino-induced processes.

Comparing our numerical results with the recent data on neutrino-induced coherent pion production, we have found that the result for the CC process is consistent with the upper limit from K2K [1] and that the result for the NC process is somewhat smaller than the preliminary experimental value from MiniBooNE [42]. However, as discussed in the literature, MiniBooNE's analysis may have overestimated the cross section owing to the use of the RS model in their analysis. We have examined to what extent the various aspects of physics involved in our model individually affect the cross sections. We have shown that the medium effect on the Δ (the spreading potential effect, in particular) and the FSI change the cross sections significantly. It is to be noted, however, that these rather drastic changes in the cross sections owing to medium effects are well under control because (i) the spreading potential and the pion distorted-wave function have been fitted to and tested by the empirical total and elastic cross sections for pion-nucleus scattering in and around the Δ region, and (ii) medium effects of a similar magnitude for the photoprocess have been shown to bring our calculation into good agreement with the data.

An interesting feature of our model is that the unitarized nonresonant amplitudes make a significant contribution to the cross sections. This is in sharp contrast with the results of previous calculations; for instance, the calculations in Refs. [7] and [16], which considered a tree-level nonresonant mechanism, found almost no contribution from it. It is worth emphasizing that this noticeable difference should not be taken as a measure of uncontrollable model dependence because (as we have confirmed) the difference arises largely from unitarization of the nonresonant amplitude, which clearly needs to be implemented.

We have re-examined the nonlocal effect in Δ propagation in nuclei. It was emphasized in Ref. [21] that this nonlocal effect, despite its large size, was not considered explicitly in any of the existing models for neutrino-induced coherent pion production (whether based on a microscopic model or the RS model). The authors of Ref. [21] made this remark based on their calculation that only included the Δ mechanism. Our present calculation, which additionally incorporates the spreading potential and FSI, also indicates that the non-locality has a large effect. Thus, regardless of the level of sophistication in the treatment of medium effects, one should always include the nonlocality effect explicitly.

Because it is expected that the SciBooNE and the Mini-BooNE collaborations will report more detailed data on (anti-) neutrino-induced coherent CC and NC pion productions, we have presented numerical results relevant to these experiments.

Finally, we have made a comparison of the elementary amplitude (HNV [47]) used by Amaro *et al.* [7] and ours (SL [17,18]) to clarify similarities and differences between them. The noteworthy points are as follows. (i) At tree level, both the SL and the HNV models have essentially the same nonresonant mechanism. (ii) In the SL model, a unitary pion production amplitude is obtained by solving the LS equation in which the tree diagrams are embedded, whereas in the HNV model, the sum of the tree diagrams is identified with the pion production amplitude. (iii) The nonresonant amplitudes of SL and HNV work differently both for the elementary processes (e.g., $\nu_\mu + p \rightarrow \mu^- + \pi^+ + p$) and for coherent pion production. (iv) In the SL model, the rescattering contribution contained in the nonresonant amplitude considerably enhances the cross section for coherent pion production.

ACKNOWLEDGMENTS

S.X.N. acknowledges informative discussions with Hidekazu Tanaka and Hirohisa Tanaka about the SciBooNE and MiniBooNE experiments. S.X.N. also thanks Akira Konaka and Issei Kato for stimulating discussions. This work was supported by the Natural Sciences and Engineering Research Council of Canada and Universidade de São Paulo (SXN), by the US Department of Energy, Office of Nuclear Physics, under Contract No. DE-AC02-06CH11357 (T.S.H.L.), by the Japan Society for the Promotion of Science, under Grant-in-Aid for Scientific Research(C) No. 20540270 (T.S.), and by the US National Science Foundation under Contract No. PHY-0758114 (K.K.).

APPENDIX A: MULTIPOLE AMPLITUDES

The amplitudes F_i^V and F_i^A in Eqs. (4) and (5) are expressed in terms of multipole amplitudes $E_{l\pm}^{V,A}$, $M_{l\pm}^{V,A}$, $S_{l\pm}^{V,A}$, and $L_{l\pm}^A$ as

$$F_1^V = \sum_l [P'_{l+1} E_{l+}^V + P'_{l-1} E_{l-}^V + l P'_{l+1} M_{l+}^V + (l+1) P'_{l-1} M_{l-}^V]. \quad (\text{A1})$$

$$F_2^V = \sum_l [(l+1) P'_l M_{l+}^V + l P'_l M_{l-}^V], \quad (\text{A2})$$

$$F_3^V = \sum_l [P''_{l+1} E_{l+}^V + P''_{l-1} E_{l-}^V - P''_{l+1} M_{l+}^V + P''_{l-1} M_{l-}^V], \quad (\text{A3})$$

$$F_4^V = \sum_l [-P''_l E_{l+}^V - P''_l E_{l-}^V + P''_l M_{l+}^V - P''_l M_{l-}^V], \quad (\text{A4})$$

$$F_5^V = \sum_l [(l+1) P'_{l+1} L_{l+}^V - l P'_{l-1} L_{l-}^V], \quad (\text{A5})$$

$$F_6^V = \sum_l [-(l+1) P'_l L_{l+}^V + l P'_l L_{l-}^V], \quad (\text{A6})$$

$$F_7^V = \sum_l [-(l+1) P'_l S_{l+}^V + l P'_l S_{l-}^V], \quad (\text{A7})$$

$$F_8^V = \sum_l [(l+1) P'_{l+1} S_{l+}^V - l P'_{l-1} S_{l-}^V], \quad (\text{A8})$$

and

$$F_1^A = \sum_l [P'_l E_{l+}^A + P'_l E_{l-}^A + (l+2) P'_l M_{l+}^A + (l-1) P'_l M_{l-}^A], \quad (\text{A9})$$

$$F_2^A = \sum_l [(l+1) P'_{l+1} M_{l+}^A + l P'_{l-1} M_{l-}^A], \quad (\text{A10})$$

$$F_3^A = \sum_l [P''_l E_{l+}^A + P''_l E_{l-}^A + P''_l M_{l+}^A - P''_l M_{l-}^A], \quad (\text{A11})$$

$$F_4^A = \sum_l [-P''_{l+1} E_{l+}^A - P''_{l-1} E_{l-}^A - P''_{l+1} M_{l+}^A + P''_{l-1} M_{l-}^A], \quad (\text{A12})$$

$$F_5^A = \sum_l [-(l+1) P'_l L_{l+}^A + l P'_l L_{l-}^A], \quad (\text{A13})$$

$$F_6^A = \sum_l [(l+1) P'_{l+1} L_{l+}^A - l P'_{l-1} L_{l-}^A], \quad (\text{A14})$$

$$F_7^A = \sum_l [(l+1) P'_{l+1} S_{l+}^A - l P'_{l-1} S_{l-}^A], \quad (\text{A15})$$

$$F_8^A = \sum_l [-(l+1) P'_l S_{l+}^A + l P'_l S_{l-}^A]. \quad (\text{A16})$$

$P_l(x)$ is the Legendre function and $x = \hat{k} \cdot \hat{q}$; \mathbf{k} and \mathbf{q} are the pion momentum and the momentum transfer to the nucleon, respectively.

The multipole amplitudes from isovector currents are further decomposed according to the total isospin (T) in the final πN state as

$$X_{l\pm}^{V,A} = \sum_{T=1/2,3/2} X_{l\pm}^{(T)V,A} \Lambda_{ij}^T, \quad (\text{A17})$$

with X being E , M , L , or S . We have introduced the projection operator Λ_{ij}^T defined by

$$\Lambda_{ij}^{3/2} = \frac{2\delta_{i,j} - i\epsilon_{ijk}\tau_k}{3}, \quad (\text{A18})$$

$$\Lambda_{ij}^{1/2} = \frac{\delta_{i,j} + i\epsilon_{ijk}\tau_k}{3}, \quad (\text{A19})$$

where the indexes i and j refer to the final pion isospin state and the component of the isovector current, respectively. For electromagnetic or NC processes, $M_{l\pm}^{(0)V} \tau_i$, which is attributable to an isoscalar current, is also added to Eq. (A17).

In the text we sometimes use the notation $X_{l\pm}^{V(A),\zeta}$, where ζ collectively denotes the pion charge and the nucleon isospin state; $X_{l\pm}^{V(A),\zeta}$ is a matrix element (in isospin space) of Eq. (A17). Because we are only concerned with coherent pion production, the specification of the pion charge determines i and j in Eq. (A17). We can find the matrix element (in isospin space) of Eq. (A17) by specifying the nucleon isospin state.

APPENDIX B: LORENTZ TRANSFORMATION FROM ACM TO 2CM

In coherent pion production in neutrino-nucleus scattering ($\nu_\ell + t \rightarrow \ell^- + \pi^+ + t$), the elementary process is $W^+(q_A) + N(p_N) \rightarrow \pi^+(k_A) + N(p'_N)$, where the four-momenta in the pion-nucleus center-of-mass frame (ACM) are given in parentheses. We suppose here that the pion momentum is on-shell. In a prescription we employ, the nucleon momenta are fixed as

$$\begin{aligned} \mathbf{p}_N &= -\frac{\mathbf{q}_A}{A} - \frac{A-1}{2A}(\mathbf{q}_A - \mathbf{k}_A), \\ \mathbf{p}'_N &= -\frac{\mathbf{k}_A}{A} + \frac{A-1}{2A}(\mathbf{q}_A - \mathbf{k}_A), \end{aligned} \quad (\text{B1})$$

and the invariant mass (W) of the pion and nucleon is

$$W = \sqrt{(p_N^0 + q_A^0)^2 - (\mathbf{p}_N + \mathbf{q}_A)^2}, \quad (\text{B2})$$

where p_N^0 is the nucleon energy on the mass shell. We note that W depends on x_A ($\equiv \hat{k}_A \cdot \hat{q}_A$) as well as $|\mathbf{q}_A|$ and $|\mathbf{k}_A|$. For convenience, we write $W(|\mathbf{q}_A|, |\mathbf{k}_A|, x_A)$.

We perform the standard Lorentz transformation from ACM to the πN CM frame (2CM). An arbitrary four-momentum in 2CM (p_2) is written with the corresponding four-momentum in ACM (p_A) as

$$\begin{aligned} p_2 &= p_A - \frac{p_A^0}{W} \mathbf{P} + \frac{P^0 - W}{W} (\mathbf{p}_A \cdot \hat{\mathbf{P}}) \hat{\mathbf{P}}, \\ p_2^0 &= \frac{P^0 p_A^0 - \mathbf{p}_A \cdot \mathbf{P}}{W}, \end{aligned} \quad (\text{B3})$$

with $\mathbf{P} = \mathbf{p}_N + \mathbf{q}_A$.

We now consider a case in which the pion momentum is off-shell (k'_A). We encounter this situation when we consider the FSI in the coherent process. As before, the nucleon momenta are fixed using Eq. (B1) with k_A replaced by k'_A . However, we do not use the nucleon energy on the mass shell. Instead, we take p_N^0 so that

$$W(|\mathbf{q}_A|, |\mathbf{k}'_A|, x'_A) = W(|\mathbf{q}_A|, |\mathbf{k}_A|, x_A) \quad \text{for } x'_A = x_A, \quad (\text{B4})$$

where W is obtained with Eq. (B2). With the nucleon four-momentum (p_N) obtained in this way, we can perform the Lorentz transformation as Eq. (B3). This prescription greatly reduces the amount of labor involved in our numerical calculation, because the SL amplitudes need to be calculated at each value of W . With the variables just obtained, we can calculate Γ_{2AL} used in Eqs. (35) and (42):

$$\Gamma_{2AL} = \sqrt{\frac{\omega'_{\pi,2} p_{N,2}^0 p_{N,2}^0}{\omega'_{\pi,A} p_{N,L}^0 p_{N,L}^0}}, \quad (\text{B5})$$

with $\omega'_{\pi,A} = \sqrt{\mathbf{k}'_A + m_\pi^2}$.

Finally, we discuss the factor Γ^χ , used in Eqs. (35) and (42), which originates from the pion wave function owing to the Lorentz transformation. Among the FSIs, the simplest process is the scattering of the pion off a single nucleon, $\pi(k'_A) + N(p'_N) \rightarrow \pi(k_A) + N(p_N)$, where the variables in ACM are shown in parentheses; only k_A is on-shell. Similarly

to Eq. (B1), we fix the nucleon momenta as

$$\begin{aligned} p''_N &= -\frac{\mathbf{k}'_A}{A} - \frac{A-1}{2A}(\mathbf{k}'_A - \mathbf{k}_A), \\ p'_N &= -\frac{\mathbf{k}_A}{A} + \frac{A-1}{2A}(\mathbf{k}'_A - \mathbf{k}_A). \end{aligned} \quad (\text{B6})$$

We assume here that the energies of all the nucleons are on the mass shell. For the Lorentz transformation from ACM to LAB specified in this way, we can calculate the Lorentz factor as

$$\Gamma^\chi = \sqrt{\frac{\omega_{\pi,A} E''_{N,A} E^f_{N,A}}{\omega_{\pi,L} E''_{N,L} E^f_{N,L}}} \simeq \sqrt{\frac{\omega_{\pi,A}}{\omega_{\pi,L}}}, \quad (\text{B7})$$

Although the actual FSI includes multiple scattering processes, it is beyond our framework to calculate Γ^χ with multiple scattering taken into account. We therefore use Γ^χ calculated for the elementary process in Eqs. (35) and (42). Actually, the Lorentz factor for the plane-wave term in Eq. (58) is given by the rightmost expression in Eq. (B7). Because the approximate equality in Eq. (B7) is quite accurate for $\mathbf{k}'_A = \mathbf{k}_A$, we use the middle expression in Eq. (B7) to evaluate the matrix elements in Eqs. (35) and (42).

APPENDIX C: EXPRESSIONS FOR SOME COMPONENTS IN THE Δ PROPAGATOR

1. Pauli correction to the Δ self-energy

We follow Ref. [26] to calculate the Pauli correction to the Δ self-energy (Σ_{Pauli}). The $\pi N \Delta$ coupling is from the SL model.

$$\begin{aligned} \Sigma_{\text{Pauli}} &= \frac{m_N}{W} \left[2\theta(k_F - \beta) \int_0^{k_F - \beta} dq q^2 \right. \\ &\quad \times \frac{\omega_\pi(q) F_{\pi N \Delta}^{\text{bare}}(q) F_{\pi N \Delta}(q)}{K^2 - q^2 + i\epsilon} \\ &\quad + \int_{|k_F - \beta|}^{k_F + \beta} dq q^2 \left(1 - \frac{q^2 + \beta^2 - k_F^2}{2q\beta} \right) \\ &\quad \left. \times \frac{\omega_\pi(q) F_{\pi N \Delta}^{\text{bare}}(q) F_{\pi N \Delta}(q)}{K^2 - q^2 + i\epsilon} \right], \end{aligned} \quad (\text{C1})$$

where $\theta(x)$ is the step function, k_F is the Fermi momentum [Eq. (31)], W is the πN invariant mass [Eq. (21)], $\omega_\pi(q) = \sqrt{q^2 + m_\pi^2}$, and

$$K^2 = \frac{m_N}{W} [(W - m_N)^2 - m_\pi^2]. \quad (\text{C2})$$

Furthermore, for electroweak pion production amplitude [Eq. (35)],

$$\boldsymbol{\beta} = \frac{m_N}{W} (\mathbf{p}_N + \mathbf{q}_A), \quad (\text{C3})$$

where \mathbf{p}_N is fixed using Eq. (20), and \mathbf{q}_A is the momentum transfer to a nucleus in ACM; for the optical potential [Eq. (52)], \mathbf{q}_A is replaced with \mathbf{k}_A (the incoming pion momentum). We use the on-shell pion momentum to fix \mathbf{p}_N . The dressed $\pi N \Delta$ vertex ($F_{\pi N \Delta}$) is taken from Eq. (14), and

the bare $\pi N\Delta$ vertex, denoted $F_{\pi N\Delta}^{\text{bare}}$, is given as [17]

$$F_{\pi N\Delta}^{\text{bare}}(q) = -i \frac{f_{\pi N\Delta}}{m_\pi} \sqrt{\frac{E_N(q) + m_N}{24\pi^2 E_N(q) \omega_\pi(q)}} \left(\frac{\Lambda_{\pi N\Delta}^2}{\Lambda_{\pi N\Delta}^2 + q^2} \right)^2 q. \quad (\text{C4})$$

2. Δ spreading potential

We consider the following spreading potential consisting of the central and the LS parts:

$$\Sigma_{\text{spr}} = V_C \frac{\rho_t(r)}{\rho_t(0)} + V_{\text{LS}} f_{\text{LS}}(r) 2\mathbf{L}_\Delta \cdot \boldsymbol{\Sigma}_\Delta, \quad (\text{C5})$$

$$f_{\text{LS}}(r) = \mu r^2 e^{-\mu r^2}, \quad (\text{C6})$$

with $\mu = 0.3 \text{ fm}^{-2}$. We have two complex coupling constants, V_C and V_{LS} , which are fitted to pion-nucleus scattering data. The radial dependence of the LS spreading potential is taken from Ref. [48]. We implement the spreading potential [Eq. (C5)] in the Δ propagator after evaluating the doorway-

state expectation value of the LS term. Thus, the LS term provides an L -dependent shift of the resonance mass and width as [48]

$$\Sigma_{\text{LS}}^L = -5V_{\text{LS}} \frac{\langle \phi_L | \rho_t f_{\text{LS}} k^2 - (\rho_t f_{\text{LS}})' \frac{d}{dr} + \frac{L(L+1)}{2r} (\rho_t f_{\text{LS}})' | \phi_L \rangle}{\langle \phi_L | \rho_t k^2 - (\rho_t)' \frac{d}{dr} | \phi_L \rangle}, \quad (\text{C7})$$

with the plane-wave pion function $\phi_L(r) = j_L(kr)$.

3. Δ (nucleon) potential

$$V_\Delta(r) = V(r) = (-55 \text{ MeV}) \left(\frac{\rho_t(r)}{\rho_t(0)} \right). \quad (\text{C8})$$

4. Δ Coulomb potential

$$V_\Delta^C(r) = \begin{cases} (r \geq R_e) & (r < R_e) \\ \left\{ \begin{array}{ll} \frac{2(Z-1)\alpha}{r}, & -\frac{(Z-1)\alpha r^2}{R_e^3} + \frac{3(Z-1)\alpha}{R_e} \quad (\pi^+ + p \rightarrow \Delta^{++}), \\ \frac{Z\alpha}{r}, & -\frac{Z\alpha r^2}{2R_e^3} + \frac{3Z\alpha}{2R_e} \quad (\pi^+ + n \rightarrow \Delta^+), \\ 0, & 0 \quad (\pi^- + p \rightarrow \Delta^0), \\ -\frac{Z\alpha}{r}, & \frac{Z\alpha r^2}{2R_e^3} - \frac{3Z\alpha}{2R_e} \quad (\pi^- + n \rightarrow \Delta^-). \end{array} \right. \end{cases} \quad (\text{C9})$$

In Eq. (C9) Z is the atomic number. The equivalent square well radius, denoted R_e , is related to the mean square

($\langle r^2 \rangle$) of a nucleus by

$$R_e = \sqrt{\frac{5}{3} \langle r^2 \rangle}. \quad (\text{C10})$$

- [1] M. Hasegawa *et al.* (K2K Collaboration), Phys. Rev. Lett. **95**, 252301 (2005).
 [2] K. Hiraide *et al.* (SciBooNE Collaboration), Phys. Rev. D **78**, 112004 (2008).
 [3] A. A. Aguilar-Arevalo *et al.* (MiniBooNE Collaboration), Phys. Lett. B **664**, 41 (2008).
 [4] V. T. McGary, in *Proceedings of 43rd Rencontres de Moriond on Electroweak Interactions and Unified Theories*; arXiv:0806.2347 [hep-ex].
 [5] H. Tanaka, in *Proceedings of Sixth International Workshop on Neutrino-Nucleus Interactions in the Few-GeV Region (NUIINT-09)*, AIP Conf. Proc. **1189**, 255 (2009).
 [6] D. Rein and L. M. Sehgal, Nucl. Phys. B **223**, 29 (1983).

- [7] J. E. Amaro, E. Hernandez, J. Nieves, and M. Valverde, Phys. Rev. D **79**, 013002 (2009).
 [8] E. Hernández, J. Nieves, and M. J. Vicente-Vacas, Phys. Rev. D **80**, 013003 (2009).
 [9] S. S. Gershtein, Yu. Ya. Komachenko, and M. Yu. Khlopov, Sov. J. Nucl. Phys. **32**, 861 (1980); Yu. Ya. Komachenko and M. Yu. Khlopov, *ibid.* **45**, 295 (1987).
 [10] P. Vilain *et al.* (CHARM II Collaboration), Phys. Lett. B **313**, 267 (1993).
 [11] D. Rein and L. M. Sehgal, Phys. Lett. B **657**, 207 (2007).
 [12] E. A. Paschos, A. Kartavtsev, and G. J. Gounaris, Phys. Rev. D **74**, 054007 (2006).
 [13] Ch. Berger and L. M. Sehgal, Phys. Rev. D **79**, 053003 (2009).

- [14] S. K. Singh, M. S. Athar, and S. Ahmad, Phys. Rev. Lett. **96**, 241801 (2006).
- [15] L. Alvarez-Ruso, L. S. Geng, and S. Hirenzaki, and M. J. Vicente Vacas, Phys. Rev. C **75**, 055501 (2007).
- [16] L. Alvarez-Ruso, L. S. Geng, and M. J. Vicente Vacas, Phys. Rev. C **76**, 068501 (2007).
- [17] T. Sato and T.-S. H. Lee, Phys. Rev. C **54**, 2660 (1996).
- [18] T. Sato, D. Uno, and T.-S. H. Lee, Phys. Rev. C **67**, 065201 (2003).
- [19] T. Sato and T.-S. H. Lee, Phys. Rev. C **63**, 055201 (2001).
- [20] B. Karaoglu and E. J. Moniz, Phys. Rev. C **33**, 974 (1986).
- [21] T. Leitner, U. Mosel, and S. Winkelmann, Phys. Rev. C **79**, 057601 (2009).
- [22] L. S. Kisslinger and W. L. Wang, Annals Phys. **99**, 374 (1976).
- [23] M. Hirata, F. Lenz, and K. Yazaki, Annals Phys. **108**, 116 (1977).
- [24] M. Hirata, J. H. Koch, E. J. Moniz, and F. Lenz, Annals Phys. **120**, 205 (1979).
- [25] S. Taniguchi, T. Sato, and H. Ohtsubo, Prog. Theor. Phys. **102**, 333 (1999).
- [26] E. J. Moniz and A. Sevgen, Phys. Rev. C **24**, 224 (1981).
- [27] J. H. Koch and E. J. Moniz, Phys. Rev. C **20**, 235 (1979); **27**, 751 (1983).
- [28] M. Gmitro, J. Kvasil, and R. Mach, Phys. Rev. C **31**, 1349 (1985).
- [29] A. A. Chumalov, R. A. Eramzhian, and S. S. Kamalov, Z. Phys. A **328**, 195 (1987).
- [30] C. W. De Jager, H. De Vries, and D. De Vries, At. Data Nucl. Data Tables **36**, 495 (1987).
- [31] P. E. Bosted, Phys. Rev. C **51**, 409 (1995).
- [32] R. A. Eisenstein and F. Tabakin, Comput. Phys. Commun. **12**, 237 (1976).
- [33] A. Kerman, H. McManus, and R. Thaler, Ann. Phys. **8**, 551 (1959).
- [34] C. M. Vincent and S. C. Phatak, Phys. Rev. C **10**, 391 (1974).
- [35] F. Binon, P. Duteil, J. P. Garron, J. Gorres, L. Hugon, J. P. Peigneux, C. Schmit, M. Spighel, and J. P. Stroot, Nucl. Phys. B **17**, 168 (1970).
- [36] M. Blecher *et al.*, Phys. Rev. C **20**, 1884 (1979).
- [37] M. J. Leitch *et al.*, Phys. Rev. C **29**, 561 (1984).
- [38] R. Gothe *et al.*, Phys. Lett. B **355**, 59 (1995).
- [39] B. Krusche *et al.*, Phys. Lett. B **526**, 287 (2002).
- [40] M. H. Ahn *et al.*, Phys. Rev. D **74**, 072003 (2006).
- [41] A. A. Aguilar-Arevalo *et al.* (MiniBooNE Collaboration), Phys. Rev. D **79**, 072002 (2009).
- [42] J. L. Raaf, Ph.D thesis, University of Cincinnati, FERMILAB-THESIS-2007-20 (2005).
- [43] I. Kato (K2K and T2K Collaborations), Nucl. Phys. B, Proc. Suppl. **168**, 199 (2007).
- [44] T. Takaki, T. Suzuki, and J. H. Koch, Nucl. Phys. A **443**, 570 (1985).
- [45] K. Hiraide, in *Proceedings of Sixth International Workshop on Neutrino-Nucleus Interactions in the Few-GeV Region (NUINT-09)*, AIP Conf. Proc. **1189**, 249 (2009).
- [46] S. Boyd, S. Dytman, E. Hernández, J. Sobczyk, and R. Tacik, in *Proceedings of Sixth International Workshop on Neutrino-Nucleus Interactions in the Few-GeV Region (NUINT-09)*, AIP Conf. Proc. **1189**, 60 (2009); Many plots are available at <http://regie2.phys.uregina.ca/neutrino>.
- [47] E. Hernández, J. Nieves, and M. Valverde, Phys. Rev. D **76**, 033005 (2007).
- [48] Y. Horikawa, M. Thies, and F. Lenz, Nucl. Phys. A **345**, 386 (1980).